Chapter 7
Particle Filter Based Integrated Health Monitoring in Bond Graph Framework

Mayank S. Jha, G. Dauphin-Tanguy, and B. Ould-Bouamama

7.1 Introduction

Besides the abrupt faults that have been considered in the previous chapters, incipient system faults and degradations of the system parameters pose significant hurdles in efficient maintenance of the system. For example, fatigue enabled wear in turbine blades, incipient leakage in valves of process engineering systems, friction induced jamming of rod in aircraft actuators, etc., pose great threat to system reliability and safety. Such problems are efficiently resolved when addressed under the realm of the so-called *condition based maintenance* (CBM) and *prognostics and health management* (PHM) [34]. The latter represent a *predictive* maintenance philosophy that has emerged only recently on contrary to the traditional strategies based upon *preventive* and *corrective* maintenance.

The main feature of CBM is the consideration of the "actual" condition of system component for designing maintenance actions rather than on an elapsed time or running hours' basis. Thus, CBM primarily depends upon current assessment of system health or state and involves real time data monitoring and processing. The two basic aspects of CBM are *diagnostics* and *prognostics.* As seen in the previous chapters, *Diagnostics* involves detection of fault and thereby, identification and quantification of the root cause of a problem. *Prognostics* involves prediction of the future health of the equipment either before or after a problem occurred [34,

M.S. Jha (✉)
Ecole Centrale de Lille, Toulouse, France
e-mail: mayank-shekhar.jha@centralelille.fr; jha.mayank.jha@gmail.com

G. Dauphin-Tanguy
Ecole Centrale de Lille, Villeneuve-d'Ascq, France

B. Ould-Bouamama
Ecole Polytech de Lille, Villeneuve d Ascq cedex, France

W. Borutzky (ed.), *Bond Graphs for Modelling, Control and Fault Diagnosis of Engineering Systems*, DOI 10.1007/978-3-319-47434-2_7

60]. As stated in [33], *prognostics* is "*estimation of time to failure and risk for one or more existing and future failure modes*."

The *Remaining Useful Life* (RUL) becomes a reliable estimate of the time to failure; it denotes how long system can function safely/reliably and within the prescribed limits of system functionalities. Thus, assessment of RUL involves predictions in future. In this context, the major motivation remains in providing sufficient lead-time between detection of a fault (diagnostic step) and occurrence of the system/component failure so that *pro-active* maintenance actions can be strategized in advance [62].

RUL prediction is not a trivial task as it involves future predictions which not only require precise information of current health, but also remain sensitive to various types of uncertainties to a large degree. These uncertainties involve stochastic evolution of incipient degradations, failure modes, varying operational conditions, measurement noise, etc. In face of all such uncertainties, the prognostic procedure must be able to accurately assess the rapidity of system degradation till failure and novel events that may significantly influence the assumed/learnt degradation trend. Due to inherent stochastic phenomena and uncertainty involved, evaluation of confidence on RUL predictions is given a significant weightage. In fact, several business decisions are based upon confidence limits associated with RUL predictions rather than the specific value of RUL itself [59]. In essence, determination of accurate and precise RUL estimate forms the core objective of any prognostics procedure.

On the other hand, the term PHM describes the systems that implement a CBM philosophy [62]. However, in the context of PHM, *prognostics* gains a wider meaning encompassing the tasks of fault detection, fault-identification, current health assessments, performance monitoring, and RUL predictions [34]. Thus, diagnostics and prognostics form building blocks of any CBM enabled PHM architecture. When these two essential tasks are achieved in an integrated manner, such a common paradigm may be given the designation of integrated health monitoring framework [9, 35].

In BG framework, diagnostics and prognostics task can be achieved in an integrated way by exploiting the properties of Analytical Redundancy Relations (ARRs) and their numerical evaluations or residuals. In this context, due to deterministic nature of ARRs, most of the existing works have neglected the inherent randomness in damage progression [20, 23, 48, 49], which in turn has led to RUL predictions that do not incorporate associated uncertainties and inherent stochasticity.

This chapter details ARR based integrated health monitoring methodology where the benefits of *BG in Linear Fractional Transformations* (BG-LFTs) have been integrated with advantages of Bayesian inference techniques to obtain accurate and precise estimate of parametric health in probabilistic domain. The inherent randomness in degradation progression is effectively managed by using sequential Monte Carlo based particle filters (PF) for estimation of state of a system parameter and subsequent RUL prediction in probabilistic domain.

After this introduction, Sect. 7.2 details various approaches of prognostics, BG-LFT method, and non-linear Bayesian inference technique using PFs. Section 7.3

discusses degradation models (DM). The method of prognostics is described in the next section. Sections 7.4 and 7.5 discuss the integrated health monitoring strategy and evaluation metrics, respectively. Section 7.6 details the application of methodology on a mechatronic system in real system. Section 7.7 draws conclusions.

7.2 Background and Techniques

This section discusses different techniques of prognostics. Moreover, BG-LFT technique of modelling uncertain systems and associated fault detection technique is discussed briefly. The latter is employed for detection of degradation initiation for the integrated health monitoring purposes. Additionally, non-linear Bayesian filtering using particle filters (PF) is described as it plays a significant role in the prognostics method presented in this chapter.

7.2.1 Approaches of Prognostics

Last decade has witnessed an extensive surge in development of various prognostics techniques and its application in diverse technical domains. Due to the inherent versatility, approaches of prognostics have been attempted to be classified in different ways [33, 34, 43, 45, 62], etc. Here, the authors have preferred to adapt the classification presented in [60].

Probabilistic Life-Usage Models These approaches depend upon the statistical information collected to assess the historical failure rate of the components and develop life-usage models [6, 30, 53]. Various functions can be applied to model statistical failure data such as exponential, normal, lognormal, and Weibull functions [39]. Moreover, the RUL is described as a *probability density function* (PDF) [60, 62]. Accurate assessment of RUL demands huge sets of failure database and extensive testing.

Data-Driven Prognostics The data associated with system functionality, degradation patterns, etc., are exploited using machine learning techniques to extract system signals and features which can be used to obtain behavior of damage progression, health index, etc. Broadly, two major strategies can be identified as discussed below.

Degradation Trend Extrapolation and Time Series Predictions In broad terms, the signals that indicate the state of the system are mapped as function of time and extrapolated in future using various techniques until a prefixed failure threshold is reached/crossed [27]. Mainly time series forecasting techniques are borrowed for this purpose such as: linear/non-linear regression techniques, autoregressive models [63], exponential smoothing techniques [10], autoregressive moving average

(ARMA), and autoregressive integrated moving average (ARIMA) [8]. The ARMA models and associated variants prove efficient for short-term predictions. Due to noise and inefficient uncertainty management, they prove less reliable for long term predictions.

Learning Damage Progression The degradation trends, failure patterns, etc., are learnt for training mathematical models. The latter in turn is used to model the relationship between damage progression and RUL. Employment of artificial neural networks (ANNs) and their numerous variants fall under this category. Feed-forward ANNs are extensively employed to estimate the current degradation index (state) by using system features (extracted signals, feature pattern, etc.) as inputs. Then, one step ahead prediction is generated by using previous state of degradation values (degradation index). The next iteration uses this prediction to produce long term predictions [31]. Major drawback in this context is that the efficiency of predictions remain limited in face of variable degradation trends, novel failure modes, etc. As such, accurate RUL predictions are not obtained on individual component unit to unit basis, but rather over large sets of component population. A comprehensive updated review of data-driven techniques can be found in [3, 61].

Model Based Prognostics Under this category, physics-of-failure models or degradation models (DM) are typically used to assess the damage progression and *state of health* (SOH). These DMs are derived from the first principles of physics. As such, they possess the capability of attaining maximum accuracy and versatility (scope of adaptation under varying degradation trend). There is a clear understanding of the underlying degradation process. There exists vast literature such as fatigue models for modelling initiation and propagation of cracks in structural components [65], electrolytic overstress aging [12], Arrhenius equation for prediction of resistance drift [41], physics-inspired power model [47] or log-linear model for degradation of current drain [46], and physics-inspired exponential degradation model for aluminum electrolytic capacitors [42].

Given the behavioral model of damage progression, the current SOH is popularly obtained in probabilistic domain with the help of Bayesian estimation techniques. Based upon the current SOH estimate, prediction of RUL is done. Such a probabilistic framework involving recursive Bayesian techniques efficiently addresses the main issues related to SOH under variable degradation; efficient management of uncertainty, environmental noise, future loading conditions, and associated confidence limits for RUL predictions [15, 16, 18, 54]. Filter for estimation and prediction process is chosen based upon the modelling hypothesis and desired performances [19]. Well-known Kalman filter, an optimal estimator for linear systems, has been used for prognostics in [12]. Extended Kalman filter (EKF) or unscented Kalman filter may also be used for joint state-parameter estimation as presented in [13, 52], respectively. However, they remain restricted to additive

Gaussian noise. Additionally, EKF being sub-optimal diverges quickly if the initial estimate of state is different from the reality by big measure or the model considered for estimation is not correct [57].

Set in Monte Carlo framework, PFs form a suitable filter choice in this context [4, 25]. PF can be applied to non-linear systems corrupted with non-Gaussian noises, for which optimal solutions may be unavailable or intractable. Comprehensive comparison of filters for prognostic purposes is found in [3, 19, 57]. Recently, PFs have been extensively for prognostic purposes [50]. Significant works include prediction of end of life (EOL) in lithium-ion batteries [55], battery health monitoring [56], prediction of battery grid corrosion [1], estimation and prediction of crack growth [11], fuel cell prognostics [37], application to damage prognostics in pneumatic valve [15, 17], estimation–prediction of wear as concurrent damage problem in centrifugal pumps with a variance control algorithm [18], employment in distributed prognosis [54], and uncertainty management for prognostics [5]. Particle filters attract considerable attention [2], owing to the ever growing efforts being made for betterment in performances and computational efficiency, such as the use of correction loops [51], fixed–lag filters [14], and kernel smoothing method [32].

The major issue in this type of approach is the accurate and reliable modelling of underlying degradation progression. Often, such accurate degradation models are not available.

Hybrid Prognostics The problem of non-availability of highly accurate degradation models is alleviated by fusing the advantages of model based and data-driven techniques. This way, there is significant amelioration in the overall prognostic approach [36, 37]. The basic philosophy remains in capturing the damage progression using DMs that can be: (1) based upon physics of failure, first principles of behavioral physics (2) derived using machine learning techniques, and (3) obtained statistically by finding a mathematical model that best fits a given set of degradation data such as linear model $D(t) = at + b$, logarithmic model $D(t) = a\ln(t) + b$, power model $D(t) = bt^a$, exponential model $D(t) = b \times e^{at}$ with $D(t)$ as an index representing the degradation (change, percentage change, etc.), and a and b as the model parameters. In this context, significant works are obtaining capacitance loss DM using non-linear least square regression [12], relevance vector machine regression performed over aging tests data [57], DM approximated by a linear part and logarithmic/exponential part [37], and residual based statistical DM [36]. Once the DM has been obtained with acceptable accuracy, recursive Bayesian techniques as discussed previously can be employed to estimate SOH and obtain subsequent RUL predictions. This way, benefits of Bayesian estimators are integrated with data-driven approaches to learn the DM as the current information arrives sequentially.

7.2.2 Prognostics in BG Framework

Almost all of the existing attempts in BG framework for prognostics have been ARR based and deterministic in nature. Moreover, DMs are considered deterministic so that the SOH and subsequent RUL predictions are obtained deterministically [20, 23, 35, 48, 49, 64]. Being restricted in deterministic domain, the randomness associated with variable damage progression, novel events, noises, etc., are simply ignored. As such, this leads to an inefficient management of the uncertainty in prognostication process and renders the RUL predictions without confidence limits. Recently, Jha et al. [36] proposed a methodology of hybrid prognostics where the benefits of Bayesian filtering techniques and BG enabled ARRs are integrated for efficient prognostics in probabilistic domain. In fact, this chapter is inspired by the work detailed in [36].

7.2.3 Bond Graph in Linear Fractional Transformations

BG-LFT is an efficient and systematic way of representing parametric uncertainty over nominal models. An uncertainty on a parameter value θ can be introduced under either an additive form or a multiplicative one, as shown in (7.1) and (7.2), respectively.

$$\theta = \theta_n \pm \Delta\theta; \qquad \Delta\theta \geq 0 \tag{7.1}$$

$$\theta = \theta_n \left(1 \pm \delta_\theta \right); \quad \delta_\theta = \frac{\Delta\theta}{\theta_n} \tag{7.2}$$

where $\Delta\theta$ and δ_θ are, respectively, the absolute and relative deviations around the nominal parametric value θ_n. When the element characteristic law is written in terms of $\frac{1}{\theta}$, (7.2) becomes:

$$\frac{1}{\theta} = \frac{1}{\theta_n} \times \left(1 + \delta_{1/\theta}\right); \quad \delta_{1/\theta} = \frac{-\Delta\theta}{\theta_n + \Delta\theta} \tag{7.3}$$

7.2.3.1 Representation on BG

The representation technique is illustrated briefly by taking a pedagogical example of R-element in *resistance* causality. The characteristic law corresponding to R-element in the linear case (see Fig. 7.1) is given as,

$$e_R = R \times f_R \tag{7.4}$$

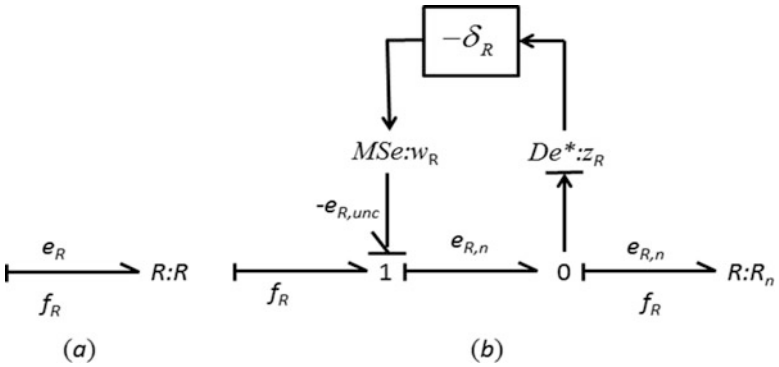

Fig. 7.1 (**a**) R-element in resistance causality. (**b**) Uncertain R-element in resistance causality in LFT form

In case of uncertainty on R, (7.4) becomes

$$e_R = R_n\,(1+\delta_R)\times f_R = R_n \times f_R + \delta_R \times R_n \times f_R = e_{Rn} + e_{Runc} \tag{7.5}$$

Constitutive Eq. (7.5) can be represented as uncertain R-element as shown in Fig. 7.1b, wherein a modulated source MSe is introduced. The latter is associated with auxiliary input w_R and a virtual effort sensor which is associated with auxiliary output z_R. It must be noted that negative (−) sign appears in the BG-LFT representation (see Fig. 7.1) due to the convention of power conservation. Moreover, the symbol De * represent virtual detectors. The virtual detectors are used to represent the information exchange/transfer.

Similarly, parametric uncertainty on the other passive elements can be represented. The technique remains similar for various other BG elements.

7.2.3.2 BG-LFT Based Robust Fault Detection

Fault diagnosis in BG-LFT framework is mainly dependent upon ARR generation [22]. ARRs are constraint relationships involving only known variables. In the context of BG modelling, an ARR : $f\big(\mathbf{SSe}(t), \mathbf{SSf}(t), \mathbf{Se}(t), \mathbf{Sf}(t), \boldsymbol{\theta}\big) = 0$, where $\boldsymbol{\theta}$ is vector of system parameters.

Generation of Uncertain ARRs The generation of robust analytical redundancy relations from an observable bond graph model is explained by the following steps:

First Step: Preferred derivative causality is assigned to the nominal model and detectors De (Df) are dualized to SSe (SSf); wherever possible. The BG-LFT model is constructed.

Second Step: The candidate ARRs are generated from "1" or "0" junction, where power conservation equation dictates that sum of efforts or flows, respectively, is equal to zero, as:

- For 0-junction:

$$\sum s_i \times f_{i,n} + \sum \mathrm{Sf} + \sum s_i w_i = 0 \tag{7.6}$$

- For 1-junction:

$$\sum s_i \times e_{i,n} + \sum \mathrm{Se} + \sum s_i w_i = 0 \tag{7.7}$$

with s being the sign rendered to the *bond* due to energy convention, w_i is the uncertain effort (flow) brought by the multiplicative parametric uncertainty δ_{θ_i} associated with ith system parameter θ_i, at 1(0) junction.

Third Step: The unknown effort or flow variables are eliminated using covering causal paths from unknown variables to known (measured) variables (dualized detectors), to obtain the ARRs which are sensitive to known variables as,

$$R = \Phi\left\{\sum \mathrm{Se}, \sum \mathrm{Sf}, \mathrm{SSe}, \mathrm{SSf}, R_n, C_n, I_n, \mathrm{TF}_n, \mathrm{GY}_n, \mathrm{RS}_n, \sum w_i\right\} \tag{7.8}$$

where subscript n represents the nominal value of the corresponding BG element.

Generation of Adaptive Thresholds The ARR derived in (7.8) consists of two perfectly separable parts due to the properties of the BG-LFT model: a nominal part noted r shown in (7.9) and an uncertain part noted $b = \sum w_i$ shown in (7.10).

$$r = \Phi\{\mathrm{Se}, \mathrm{Sf}, \mathrm{SSe}, \mathrm{SSf}, R_n, C_n, I_n, \mathrm{TF}_n, \mathrm{GY}_n, \mathrm{RS}_n\} \tag{7.9}$$

$$\begin{aligned} b &= \sum w_i \\ w_i &= \Phi\{\mathrm{Se}, \mathrm{Sf}, \mathrm{SSe}, \mathrm{SSf}, R_n, C_n, I_n, \mathrm{TF}_n, \mathrm{GY}_n, \mathrm{RS}_n, \delta_R, \delta_I, \delta_C, \delta_{\mathrm{TF}}, \delta_{\mathrm{GY}}, \delta_{\mathrm{RS}}\} \end{aligned} \tag{7.10}$$

The uncertain part generates the adaptive threshold over the nominal part. From (7.8), (7.9), and (7.10), following may be obtained:

$$\begin{aligned} r + b &= 0 \\ r &= -b = -\sum w_i \end{aligned} \tag{7.11}$$

The thresholds are formed in form of envelop as:

$$-a < r < a \tag{7.12}$$

where

$$a = \sum |w_i| \tag{7.13}$$

The use of absolute values to generate the thresholds of normal operation ensures the robustness of this algorithm to false alarms. BG-LFT technique is well developed and detailed in literature. Readers are referred to [21, 22] for details.

7.2.4 Non-Linear Bayesian Inference Using Particle Filters

Consider a dynamic system whose state at time step t_k is represented by the vector $\mathbf{x}_k$. The evolution of the system state is described by a state space model,

$$\mathbf{x}_k = \boldsymbol{f}_k\left(\mathbf{x}_{k-1}, \boldsymbol{v}_{k-1}\right) \tag{7.14}$$

$$\mathbf{y}_k = \boldsymbol{h}_k\left(\boldsymbol{x}_k, \mathbf{w}_k\right) \tag{7.15}$$

where

- $\mathbf{f}_k : \mathbb{R}^{N_x} \times \mathbb{R}^{N_v} \rightarrow \mathbb{R}^{N_x}$ is a non-linear state transition function.
- $\boldsymbol{h}_k : \mathbb{R}^{N_x} \times \mathbb{R}^{N_w} \rightarrow \mathbb{R}^{N_y}$ is observation function describing the sequence of measurements $\mathbf{y}_k$, obtained sequentially at successive time steps t_k.
- $\boldsymbol{v}_k \in \mathbb{R}^{N_v}$ is the process noise sequence of known distribution assumed *independent and identically distributed* (i.i.d).
- $\boldsymbol{w}_k \in \mathbb{R}^{N_w}$ is i.i.d measurement noise sequence of known distribution.

Equations (7.14) and (7.15) can be equivalently represented as,

$$\mathbf{x}_k = \boldsymbol{f}_k\left(\mathbf{x}_{k-1}, \boldsymbol{v}_{k-1}\right) \leftrightarrow p\left(\mathbf{x}_k \middle| \mathbf{x}_{k-1}\right) \tag{7.16}$$

$$\mathbf{y}_k = \boldsymbol{h}_k\left(\mathbf{x}_k, \boldsymbol{w}_k\right) \leftrightarrow p\left(\mathbf{y}_k \middle| \mathbf{x}_{k-1}\right) \tag{7.17}$$

where $p\left(\boldsymbol{x}_k \middle| \boldsymbol{x}_{k-1}\right)$ represents the state transition probability, $p\left(\mathbf{y}_k \middle| \mathbf{x}_{k-1}\right)$ is the likelihood function which signifies the probability of the observation of $\mathbf{y}_k$, given the current estimate of $\boldsymbol{x}_k$.

Objective of filtering procedure is to obtain estimates of $\mathbf{x}_k$, based upon all of the available measurement sequences $\mathbf{y}_{1:k} = \{\mathbf{y}_k, k = 1, 2, ...k\}$. From the perspectives of Bayesian inference, the objective remains in recursive calculation of state distribution $\mathbf{x}_k$, given the set of observations $\mathbf{y}_{1:k}$ up to time t_k, with some degree of belief. Construction of PDF $p\left(\mathbf{x}_k \middle| \mathbf{y}_{1:k}\right)$, known as the filtered *posterior state* PDF, provides all the information about $\mathbf{x}_k$, inferred from the measurements $\mathbf{y}_{1:k}$ and the initial state PDF $p(\mathbf{x}_0)$. The latter $p(\mathbf{x}_0)$ is assumed to be known. Given

$p\left(\mathbf{x}_{k-1}\middle|\mathbf{y}_{1\ :\ k-1}\right)$ at time t_{k-1}, theoretically, the posterior state can be estimated in a recursive way via two sequential steps: *prediction* and *update*.

Prediction Application of Chapman–Kolmogorov equation over $p\left(\mathbf{x}_{k-1}\middle|\mathbf{y}_{1\ :\ k-1}\right)$ at time k–1 gives the estimation of *prior* state PDF $p\left(\mathbf{x}_{k}\middle|\mathbf{y}_{1\ :\ k-1}\right)$ at time t_k as,

$$\begin{aligned} p\left(\mathbf{x}_{k}\middle|\mathbf{y}_{1\ :\ k-1}\right) &= \int p\left(\mathbf{x}_{k}\middle|\mathbf{x}_{k-1},\mathbf{y}_{1\ :\ k-1}\right) p\left(\mathbf{x}_{k-1}\middle|\mathbf{y}_{1\ :\ k-1}\right) \\ &= \int p\left(\mathbf{x}_{k}\middle|\mathbf{x}_{k-1}\right) p\left(\mathbf{x}_{k-1}\middle|\mathbf{y}_{1\ :\ k-1}\right) d\mathbf{x}_{k-1} \end{aligned} \tag{7.18}$$

Here, $p\left(\mathbf{x}_{k}\middle|\mathbf{x}_{k-1}\right)$ is obtained from (7.16), where the system is assumed to follow first order Markov dynamics.

Update Bayes rule is used to *update* the *prior* as the new measurement $\mathbf{y}_k$ arrives, to obtain the *posterior* distribution of $\mathbf{x}_k$ as,

$$p\left(\mathbf{x}_{k}\middle|\mathbf{y}_{1\ :\ k}\right) = \frac{p\left(\mathbf{x}_{k}\middle|\mathbf{y}_{1\ :\ k-1}\right) p\left(\mathbf{y}_{k}\middle|\mathbf{x}_{k}\right)}{p\left(\mathbf{y}_{k}\middle|\mathbf{y}_{1\ :\ k-1}\right)} \tag{7.19}$$

with the normalizing constant being,

$$p\left(\mathbf{y}_{k}\middle|\mathbf{y}_{1\ :\ k-1}\right) = \int p\left(\mathbf{x}_{k}\middle|\mathbf{y}_{1\ :\ k-1}\right) p\left(\mathbf{y}_{k}\middle|\mathbf{x}_{k}\right) d\mathbf{x}_{k} \tag{7.20}$$

This step incorporates the latest measurement into a priori state PDF $p\left(\mathbf{x}_{k}\middle|\mathbf{y}_{1\ :\ k-1}\right)$ to estimate the *posterior* state PDF $p\left(\mathbf{x}_{k}\middle|\mathbf{y}_{1\ :\ k}\right)$. The exact Bayesian solution obtained from recurrence relations (7.18) and (7.19) forms the basis of optimal Bayesian inference. This procedure remains tractable and produces best results for ideal systems such as linear Gaussian state space models. For the latter, it leads to the formation of classical Kalman filter. In general, optimal and closed form solutions for non-linear systems with non-Gaussian noises cannot be analytically determined. For non-linear state space models with additive Gaussian noises, sub-optimal Extended Kalman filter (EKF) has been developed. To obtain optimal solutions for non-linear systems, one resorts to Monte Carlo Methods. One such popular method is described below.

Particle filter (PF) is a type of Sequential Monte Carlo method [25], used for obtaining recursive Bayesian inferences via Monte Carlo simulations. Basic philosophy rests in representing the *posterior* state PDF by a set of random samples or "particles" where each of the particles has an associated weight based upon which the stateestimates are computed [26]. *Sequential importance sampling* (SIS) PF is

one of the most popular PFs in which posterior state PDF $p\left(\mathbf{x}_{0:k}\middle|\mathbf{y}_{1:k}\right)$ by a set of N number of weighted particles [4],

$$\left\{\left(\mathbf{x}_{0:k}^{i}\right), \mathrm{w}_{k}^{i}\right\}_{i=1}^{N} \tag{7.21}$$

where $\left\{\mathbf{x}_{0:k}^{i}, i = 1, \ldots N\right\}$ is the set of particles representing the state value with corresponding associated importance weights as $\left\{w_{k}^{i}, i = 1, \ldots N\right\}$. Moreover, $\mathbf{x}_{0\ :\ k} = \left\{\mathbf{x}_{j}, j = 0, ..., k\right\}$ is the set of all states up to time k. It should be noted that these weights are the approximations of relative posterior probabilities of the particles normalized such that,

$$\sum_{i} w^{i}{}_{k} = 1 \tag{7.22}$$

The posterior PDF is approximated as,

$$p\left(\mathbf{x}_{0:k}\middle|\mathbf{y}_{1\ :\ k}\right) \approx \sum_{i=1}^{N} \mathrm{w}_{k}^{i} \times \delta\left(\mathbf{x}_{0:k} - \mathbf{x}_{0:k}^{i}\right) \tag{7.23}$$

where δ denotes the Dirac delta function. This gives discrete weighted approximation to the true posterior state distribution $p\left(\mathbf{x}_{0:k}\middle|\mathbf{y}_{1\ :\ k}\right)$. As N tends to large numbers, the Monte Carlo approximation becomes an equivalent representation to the posterior state PDF.

7.2.5 *Importance Sampling*

Obtaining the particle weight(s) is not a trivial task. It becomes virtually impossible to sample from a posterior state $p\left(\mathbf{x}_{0:k}\middle|\mathbf{y}_{1\ :\ k}\right)$ without a closed form distribution. To resolve this issue, principle of *importance sampling* is used [4]. Here, a proposal distribution $q(x)$, known as *importance density*, is chosen such that $p(x) \propto q(x)$ and $q(x)$ is a PDF from which samples can be easily drawn. For example, if a set of samples $x^{i} \sim q(x),\ i = 1, \ldots, N$ is generated from the proposal distribution $q(x)$, then the weighted approximation of the density $p(x)$ is given as,

$$p(x) \approx \sum_{i=1}^{N} \mathrm{w}^{i} \times \delta\left(x - x^{i}\right) \tag{7.24}$$

where normalized weight can be obtained as,

$$\mathrm{w}^i \approx \frac{p\left(x^i\right)}{q\left(\mathrm{x}^i\right)} \tag{7.25}$$

For a set of samples $\left\{\mathbf{x}_{0:k}^i, i = 1, \ldots N\right\}$, this leads to weights being defined as,

$$\mathrm{w}_k^i \propto \frac{p\left(\mathbf{x}_{0:k}\middle|\mathbf{y}_{1:k}\right)}{q\left(\mathbf{x}_{0:k}\middle|\mathbf{y}_{1:k}\right)} \tag{7.26}$$

For online implementation, a recursive estimation procedure is sought. In other words, distribution $p\left(\mathbf{x}_{0:k}\middle|\mathbf{y}_{1:k}\right)$ at time t_k must be estimated from $p\left(\mathbf{x}_{0:k-1}\middle|\mathbf{y}_{1:k-1}\right)$ at time t_{k-1}, in a sequential manner. To this end, a constraint on *importance density* is placed so that it is factorable as,

$$q\left(\mathbf{x}_{0:k}\middle|\mathbf{y}_{1\ :\ k}\right) = q\left(\mathbf{x}_k\middle|\mathbf{x}_{0:k-1}, \mathbf{y}_{1\ :\ k}\right) q\left(\mathbf{x}_{0:k-1}, \mathbf{y}_{1\ :\ k-1}\right) \tag{7.27}$$

Then, the new state $\mathbf{x}_{0:k}^i \sim q\left(\mathbf{x}_k\middle|\mathbf{x}_{0:k-1}, \mathbf{y}_{1:k}\right)$ can be appended with existing samples $\mathbf{x}_{0:k-1}^i \sim q\left(\mathbf{x}_{0:k-1}\middle|\mathbf{y}_{1:k-1}\right)$ to obtain new sets of samples $\mathbf{x}_{0:k}^i \sim q\left(\mathbf{x}_{0:k}\middle|\mathbf{y}_{1:k}\right)$. This is followed by update of particle weights. The posterior state PDF is expressed as,

$$p\left(\mathbf{x}_{0:k}\middle|\mathbf{y}_{1\ :\ k}\right) = p\left(\mathbf{x}_{0:k-1}\middle|\mathbf{y}_{0\ :\ k-1}\right) \frac{p\left(\mathbf{y}_k\middle|\mathbf{x}_k\right) p\left(\mathbf{x}_k\middle|\mathbf{x}_{k-1}\right)}{p\left(\mathbf{y}_k, \mathbf{y}_{1\ :\ k-1}\right)} \tag{7.28}$$

Then, using (7.26), (7.27), and (7.28), particles are updated recursively as,

$$\begin{aligned}
\mathrm{w}_k^i &\propto \frac{p\left(\mathbf{x}_{0:k}\middle|\mathbf{y}_{1:k}\right)}{q\left(\mathbf{x}_{0:k}\middle|\mathbf{y}_{1:k}\right)} \\
&\propto \frac{p\left(\mathbf{x}_{0:k-1}\middle|\mathbf{y}_{0\ :\ k-1}\right) p\left(\mathbf{y}_k\middle|\mathbf{x}_k\right) p\left(\mathbf{x}_k\middle|\mathbf{x}_{k-1}\right)}{q\left(\mathbf{x}_k\middle|\mathbf{x}_{0:k-1}, \mathbf{y}_{1\ :\ k}\right) q\left(\mathbf{x}_{0:k-1}, \mathbf{y}_{1\ :\ k-1}\right)} \\
&\propto \mathrm{w}_{k-1}^i \frac{p\left(\mathbf{y}_k\middle|\mathbf{x}_k\right) p\left(\mathbf{x}_k\middle|\mathbf{x}_{k-1}\right)}{q\left(\mathbf{x}_k\middle|\mathbf{x}_{0:k-1}, \mathbf{y}_{1\ :\ k}\right)}
\end{aligned} \tag{7.29}$$

In SIS PF, the *importance density* is set equal to a priori PDF of state, i.e., $q\left(\mathbf{x}_{0\ :\ k}\middle|\mathbf{x}_{0\ :\ k-1}\right) = p\left(\mathbf{x}_k\middle|\mathbf{x}_{k-1}\right) = f_k\left(\mathbf{x}_k\middle|\mathbf{x}_{k-1}\right)$. This translates to the fact that

new particles can be generated from the previous set of particle by simulating the state transition function $f_k\left(\mathbf{x}_k\middle|\mathbf{x}_{k-1}\right)$. Moreover, assumption of Markov dynamics implies that $q\left(\mathbf{x}_k^i\middle|\mathbf{x}_{0:k-1}^i,\mathbf{y}_{1\ :\ k}\right)=q\left(\mathbf{x}_k^i\middle|\mathbf{x}_{k-1}^i,\mathbf{y}_k\right)$. This renders the whole procedure suitable for online implementation as only the filtered estimate $p\left(\mathbf{x}_k\middle|\mathbf{y}_{1:k}\right)$ is required at each step. Thus, only $\mathbf{x}_k^i$ and $\mathbf{y}_{1:k}$ should be stored and the previous state path up to $\mathbf{x}_{0:k-1}^i$ can be neglected. Weight update step (7.29) can be modified as,

$$\begin{aligned}\mathrm{w}_k^i &\propto \mathrm{w}_{k-1}^i\frac{p\left(\mathbf{y}_k\middle|\mathbf{x}_k^i\right)p\left(\mathbf{x}_k^i\middle|\mathbf{x}_{k-1}^i\right)}{q\left(\mathbf{x}_k^i\middle|\mathbf{x}_{0:k-1}^i,\mathbf{y}_{1\ :\ k}\right)}\\ &\propto \mathrm{w}_{k-1}^i\ p\left(\mathbf{y}_k\middle|\mathbf{x}_k^i\right)\end{aligned} \tag{7.30}$$

Then, the posterior filtered PDF $p\left(\mathbf{x}_k\middle|\mathbf{y}_{1:k}\right)$ is approximated as,

$$p\left(\mathbf{x}_k\middle|\mathbf{y}_{1\ :\ k}\right)\approx\sum_{i=1}^{N}\mathrm{w}_k^i\times\delta\left(\mathbf{x}_{0:k}-\mathbf{x}_{0:k}^i\right) \tag{7.31}$$

This simplified algorithm can be used for recursive estimation of state as the observations arrive sequentially. The likelihood functions of the new observations $p\left(\mathbf{y}_k\middle|\mathbf{x}_k^i\right)$ result in evaluation of weights of particles constituting the next state estimate.

7.2.6 *Particle Degeneracy and Resampling*

During the propagation steps, the approximation density is adjusted through reweighting of the particles. Previous steps lead to an inevitable situation where due to increase in weight variance, the importance weights become increasingly skewed. After few iterations, all but one particle have negligible weights (particle *degeneracy*) [26]. To avoid the latter, a new swarm of particles are resampled from the approximate *posterior* distribution obtained previously in the *update* stage, constructed upon the weighted particles [44]. The probability for a particle to be sampled remains proportional to its weight. This way, particles with smaller weights (signifying less contribution to estimation process) are discarded and particles with large weights are used for resampling. To resolve this issue, the standard SIS is accompanied by a *resampling* step (referred to as *Sampling-Importance resampling*) (SIR) PF [4]. The different ways of *resampling* can be referred in [24]. In this work, SIR PF is employed for estimation of SOH and RUL predictions. In general, the particles are forced in the region of high likelihood by multiplying high weighted

particles and abandoning low weighted particles. In other words, *resampling* step involves elimination of those particles that have small weights so that focus shifts on the particles with large weight. This step results in generation of a new set of particles $\left\{\left(\mathbf{x}_{0:k}^{i*}\right), \mathrm{w}_k^i\right\}_{i=1}^N$ by resampling N times without *replacement* from the discrete approximation of $p\left(\mathbf{x}_k \middle| \mathbf{y}_{1\ :\ k}\right)$ as,

$$p\left(\mathbf{x}_k \middle| \mathbf{y}_{1\ :\ k}\right) \approx \sum_{i=1}^{N} \mathrm{w}_k^i \times \delta_{(\mathbf{x}_{0:k})}\left(d\mathbf{x}_{0\ :\ k}\right) \tag{7.32}$$

such that $Pr\left(\mathbf{x}_k^{i*} = \mathbf{x}_k^i\right) = w_k^i$. The new set of particles represents i.i.d from (7.32) and thus, the particle weights are reset again as $w_k^i = 1/N$.

7.3 Degradation Models

DMs capture the underlying degradation of a given component/subsystem with time, environmental and operational conditions, etc. DMs can be obtained based upon physics of degradation or statistical approaches [28, 29]. Given a prognostic candidate (system parameter) θ^d, the associated DM can be expressed as,

$$\theta^d(t) = g^d\left(\boldsymbol{\gamma}^d(t), \boldsymbol{v}^{\theta^d}(t)\right) \ ; \qquad \theta^d\left(t=0\right) = \theta_n^d \tag{7.33}$$

where $g^d(.)$ denotes the linear/non-linear *degradation progression function* (DPF) obtained from the corresponding DM. It models the degradation progression of $\theta^d(t)$. Moreover, $\boldsymbol{\gamma}^d(t) \in \mathbb{R}^{N_{\gamma^d}}$ presents the vector of *degradation progression parameters* (DPP), $\boldsymbol{v}^{\theta^d}(t) \in \mathbb{R}^{N_{\theta^d}}$ is the associated process noise vector and θ_n^d denotes nominal value of θ^d.

7.3.1 Obtaining Degradation Model in BG Framework

In BG framework, the DM of a system parameter $\theta^d \in \boldsymbol{\theta}$, $\boldsymbol{\theta} \in \mathbb{R}^{N_\theta}$ can be obtained from the time evolution profile of the respective ARR to which it is sensitive, assuming that the rest of the system parameters sensitive to the same ARR do not undergo any kind of progressive fault or degradation [7, 49]. Here, consider the point valued part of the dth I-ARR, $r^d(t)$ such that with $\boldsymbol{\theta}' = \boldsymbol{\theta} \backslash \theta^d(t)$, $t > 0$, $r^d(t) \neq 0$,

$$r^d(t) = \Psi_1^d\left(\theta^d(t), \boldsymbol{\theta}_n', \mathbf{SSe}(t), \mathbf{SSf}(t), \boldsymbol{Se}(t), \boldsymbol{Sf}(t)\right) \tag{7.34}$$

where subscript n denotes nominal value. The computed values of $r^d(t)$ at time sample points gives an implicit relation of the degradation profile of $\theta^d(t)$ in time.

Assuming that *implicit function theorem* is satisfied [40], (7.34) gives a real valued function ψ_d such that,

$$\theta^d(t) = \psi_d\left(r^d(t), \boldsymbol{\theta}'_n, \mathbf{SSe}(t), \mathbf{SSf}(t), \boldsymbol{Se}(t), \boldsymbol{Sf}(t)\right) \tag{7.35}$$

Equation (7.35) is a function of system measurements inputs (known variables), signal derivative(s), etc., it is always corrupted with noise. It should be noted that residual based DM should be obtained prior to prognostics. This routine can be performed offline, i.e., prior to the phase when system's health monitoring is of interest.

7.3.2 Methodology of Hybrid Prognostics

In this section, the methodology for prognostics is described. Following assumptions are made:

- Only system parameters are considered uncertain. Sensors are considered non-faulty.
- A single system parameter (prognostics candidate) is assumed to be under progressive degradation. In fact, it is assumed that single mode of degradation affects the system parameter.
- The system parameter (prognostics candidate) that undergoes degradation is assumed to be known a priori. The issue of isolation or isolability of the prognostic (faulty) candidate is assumed resolved. Let $\theta^d(t) \in \boldsymbol{\theta}$ be such prognostic candidate.
- Degradation model (DM) of $\theta^d(t) \in \boldsymbol{\theta}$ is assumed to be known a priori.
- For an ARR derived, only one system parameter sensitive to it (known a priori) varies with time.
- Noise associated with measurements (residuals) is assumed normally distributed Gaussian in nature.

  Objectives are
- Reliable estimation of prognostic candidate's SOH and state of hidden degradation parameters that accelerate or vary the degradation progression.
- Reliable prediction of the RUL of the prognostic candidate.

7.3.3 Robust Detection of Degradation Initiation

The problem of detecting the degradation beginning is treated as robust fault detection problem. The BG-LFT enabled fault detection method presented in Sect. 7.2.3 is exploited in the form of an efficient diagnostic module. To this end, following steps are taken.

Table 7.1 Detection of degradation

Algorithm 1: Detection of degradation initiation
Input: $r^d(k)$, $\sum \lvert w_i(t) \rvert$
Output: ***degradation detection***
if $r^d(k) \geq -\sum \lvert w_i(t) \rvert$ **and** $r^d(k) \leq \sum \lvert w_i(t) \rvert$
degradation detection ← **false**
else
degradation detection ← **true**
end if

Step 1: Preferred derivative causality is assigned to nominal model and sensors are dualized.
Step 2: BG-LFT model of the nominal system is obtained.
Step 3: ARR sensitive to θ^d is derived. Let the ARR be $R(t)$ and the associated residual (numerical evaluation of ARR) be $r^d(t)$.
Step 4: Robust thresholds are derived as explained in Sect. 7.2.3. Degradation initiation is detected when the residual goes out of the BG-LFT thresholds. The corresponding pseudo algorithm is given in Table 7.1.

7.3.4 Fault Model Construction

This section describes the fault model constructed for estimating the state of the prognostic candidate which denotes the state of health of the parameter.

7.3.4.1 State Equation

The parameter under degradation $\theta^d(t)$ is included as a tuple $(\theta^d, \boldsymbol{\gamma}^d, g^d)$ to model the damage progression in state space form. Here, $\boldsymbol{\gamma}^d(t) \in \mathbb{R}^{N_{\gamma^d}}$ is the vector of hidden parameters (DPP) that influence the speed of degradation significantly. The *fault model* for is constructed in state space form by considering the parameter θ^d as the state variable augmented with the DPP vector as,

$$\dot{\boldsymbol{x}}^d(t) = \boldsymbol{f}^d\left(\boldsymbol{x}^d(t), \boldsymbol{v}^{x_d}(t)\right) \tag{7.36}$$

where $\boldsymbol{x}^d(t) = \left[\theta^d(t),\ \boldsymbol{\gamma}^d(t)\right]^T$ is the augmented state vector, $\mathtt{f}^d$ is state transition function following the Markov dynamics, and $\boldsymbol{v}^{\boldsymbol{x}_d} \in \mathbb{R}^{N_{v^d}}$ is the process noise vector.

7.3.4.2 ARR Based Observation Equation

The nominal residual used for detection of degradation initiation can be further exploited used for SOH estimation if the corresponding ARR expression is altered to obtain the observation equation. To this end, following theorem is enunciated:

Theorem *Under the single degradation hypothesis, assuming that the nominal part $r_n^d(t)$ of an ARR derived from the BG-LFT model can be expressed as a linear combination of non-linear functions of degradation candidate parameter $\theta^d(t)$, the measurement of the $\theta^d(t)$ can be obtained from $r_n^d(t)$.*

Proof Let $\theta^d(t)$ be the degradation candidate and $\boldsymbol{\theta}' = \boldsymbol{\theta} \backslash \theta^d(t)$. Assuming the nominal part $r_n^d(t)$ can be expressed as,

$$r_n^d(t) = \Xi\left(\boldsymbol{\theta}_n', \boldsymbol{SSe}(t), \boldsymbol{SSf}(t), \boldsymbol{Se}(t), \boldsymbol{Sf}(t)\right) + A^T \boldsymbol{\varphi}\left(\theta_n^d\right) \tag{7.37}$$

where $\forall i \Big| i = 1, 2 \ldots m, A^{m\times 1} = [a_1 \;\; a_2 \ldots a_m]^T$ is a vector of known (measured system variables) with $a_i = \phi_i\left(\boldsymbol{\theta}_n{}', \mathrm{SSe}(t), \boldsymbol{SSf}(t), \boldsymbol{Se}(t), \boldsymbol{Sf}(t)\right)$ and $\boldsymbol{\varphi}^{m\times 1}\left(\theta^d(t)\right) = \left[\varphi_1\left(\theta^d(t)\right), \varphi_2\left(\theta^d(t)\right), \ldots . \varphi_m\left(\theta^d(t)\right)\right]^T$ is the vector of non-linear functions of $\theta^d(t)$. Then, $\forall t \geq 0$ power conservation at the BG *junction* where the corresponding ARR is derived, gives

$$\mathrm{ARR}: r^d(t) = \Xi\left(\boldsymbol{\theta}_n', SSe(t), \boldsymbol{SSf}(t), \boldsymbol{Se}(t), \boldsymbol{Sf}(t)\right) + A^T \boldsymbol{\varphi}\left(\theta^d(t)\right) = 0 \tag{7.38}$$

or,

$$\begin{aligned} r^d(t) &= \Xi\left(\boldsymbol{\theta}_n', \mathbf{SSe}(t), \mathbf{SSf}(t), \sum Se, \sum Sf, \right) \\ &\quad + A^T \boldsymbol{\varphi}\left(\theta_n^d\right) + \left(A^T \boldsymbol{\varphi}\left(\theta^d(t)\right) - A^T \boldsymbol{\varphi}\left(\theta_n^d\right)\right) = 0 \\ r^d(t) &= r_n^d(t) + A^T\left(\boldsymbol{\varphi}\left(\theta^d(t)\right) - \boldsymbol{\varphi}\left(\theta_n^d\right)\right) = 0 \\ r_n^d(t) &= -\; A^T\left(\boldsymbol{\varphi}\left(\theta^d(t)\right) - \boldsymbol{\varphi}\left(\theta_n^d\right)\right) \end{aligned} \tag{7.39}$$

Thus, state of $\theta^d(t)$ can be linked implicitly with measurements obtained by the nominal part $r_n^d(t)$.

Corollary *When $\boldsymbol{\varphi}\left(\theta_n^d\right) = \varphi\left(\theta_n^d\right) = \theta_n^d$, the vector $A = a_1$, $a_1 = \phi_1\left(\boldsymbol{\theta}_n', \mathbf{SSe}(t), \mathbf{SSf}(t), \sum \mathrm{Se}, \sum \mathrm{Sf}\right)$, can be understood as a coefficient function linking the fault value to the residual. It can be found as,*

$$a_1 = \frac{\partial\left(r_n^d(t)\right)}{\partial\left(\theta^d(t)\right)} \tag{7.40}$$

Thus, observation equation can be formed as,

$$y^d(t) = r_n^d(t) = -A^T\left(\boldsymbol{\varphi}\left(\theta^d(t)\right) - \boldsymbol{\varphi}\left(\theta_n^d\right)\right) \tag{7.41}$$

In this work noise is considered additive, i.i.d., drawn from a zero mean normal distribution and is assumed uncorrelated to $\boldsymbol{x}^d(t)$. Observation equation is formed from (7.41) as,

$$y^d(t) = h^d\left(\boldsymbol{x}^d(t)\right) + w^d(t) \tag{7.42}$$

where $h_d(\cdot)$ is a non-linear observation function obtained from (7.41) and $w^d(t) \sim \mathcal{N}\left(0, \sigma_{w^d}^2\right)$. Moreover, the standard deviation σ_{w^d} is approximated from residual measurements during the degradation tests.

Thus, the nominal residual can provide information of damage and SOH of the prognostic candidate.

7.3.5 State of Health Estimation

In discrete time step $k \in \mathbb{N}$, the fault model can be described as,

$$\boldsymbol{x}_k^d = \boldsymbol{f}_k^d\left(\boldsymbol{x}_{k-1}^d, \boldsymbol{v}_{k-1}^{\boldsymbol{x}_d}\right) \tag{7.43}$$

$$y_k^d = \boldsymbol{h}_k^d\left(\boldsymbol{x}_k^d\right) + w_k^d \tag{7.44}$$

The initial state PDF $p\left(\theta_{k-1}^d, \boldsymbol{\gamma}_{k-1}^d \middle| y_{k-1}^d\right)$ is assumed to be known a priori. Estimations of θ_k^d, $\boldsymbol{\gamma}_k^d$ are obtained Bayesian framework as explained in Sect. 7.2.4. The latter is obtained as PDF $p\left(\theta_k^d, \boldsymbol{\gamma}_k^d \middle| y^d{}_{0:\ k}\right)$, at discrete time k, based upon the history of measurements till time k, $y_{0:\ k}^d$.The arriving measurement y_k^d is assumed conditionally independent of the state process. The likelihood function becomes as,

$$p\left(y_k^d \middle| \theta_k^d,\ \boldsymbol{\gamma}_k^d\right) = \frac{1}{\sigma_{w_k^d}\sqrt{2\pi}} \exp\left(-\left(y_k^d - h^d\left(x_k^d\right)\right)^2 / 2\sigma_{w_k^d}^2\right) \tag{7.45}$$

Estimation procedure using PF (see Sect. 7.2.4) is carried out such that the state PDF is approximated by set of discrete weighted samples or particles, $\left\{\left(\theta_k^{d,i},\ \boldsymbol{\gamma}_k^{d,i}\right), \mathrm{w}_k^i\right\}_{i=1}^N$, where N is the total number of particles. For ith particle at time k, $\theta_k^{d,i}$ $\boldsymbol{\gamma}_k^{d,i}$ are the joint estimate of the state. In PF, the posterior density at any time step k is approximated as,

$$p\left(\theta_k^d, \boldsymbol{\gamma}_k^d \middle| y_{0\ :\ k}^d\right) \approx \sum_{i=1}^{N} \mathrm{w}_k^i \times \delta_{\left(\theta_k^d, \boldsymbol{\gamma}_k^d\right)}\left(d\theta_k^d\ \ d\boldsymbol{\gamma}_k^d\right) \tag{7.46}$$

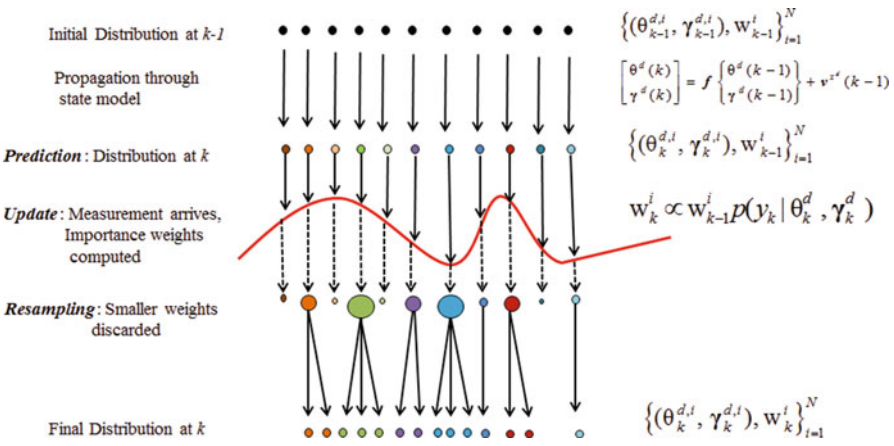

Fig. 7.2 Illustration of estimation process in particle filters

where $\delta_{\left(\theta_k^d, \boldsymbol{\gamma}_k^d\right)}\left(d\theta_k^d \;\; d\boldsymbol{\gamma}_k^d\right)$ denotes the Dirac delta function located at $(\theta_k^d, \boldsymbol{\gamma}_k^d)$ and sum of the weights $\sum_{i=1}^{N} w_k^i = 1$. In this work, SIR PF is employed, owing to the easiness of importance weight evaluation [4]. Firstly, it is assumed that the set of random samples (particles) $\left\{\left(\theta_{k-1}^{d,i}, \;\; \boldsymbol{\gamma}_{k-1}^{d,i}\right), \mathrm{w}_{k-1}^i\right\}_{i=1}^{N}$ are available as the realizations of posterior probability $p\left(\theta_{k-1}^d, \boldsymbol{\gamma}_{k-1}^d \middle| y_{0\;:\;k-1}^d\right)$ at time $k-1$. Then, three significant steps are followed as illustrated in Fig. 7.2.

Prediction The particles are propagated through system model by: sampling from the system noise $\boldsymbol{v}_{k-1}^{\boldsymbol{x}_d}$ and simulation of system dynamics shown in (7.43).

This leads to new set of particles which are nothing but the realizations of prediction distribution $p\left(\theta_k^d, \boldsymbol{\gamma}_k^d \middle| y_{0\;:\;k-1}^d\right)$.

Update As the new measurement y_k^d arrives, a weight w_k^i is associated with each of the particles based on the likelihood of observation y_k^d made at time k as,

$$w_k^i = p\left(y_k^d \middle| \theta_k^{d,i}, \boldsymbol{\gamma}_k^{d,i}\right) \Big/ \sum_{j=1}^{N} p\left(y_k^d \middle| \theta_k^{d,j}, \boldsymbol{\gamma}_k^{d,j}\right) \tag{7.47}$$

Resampling There exist many types of resampling techniques [24]. In this work, *systematic resampling* is preferred owing to its simplicity in implementation, $O(N)$ computational time, and modular nature. The *resampling* method is well detailed in literature and thus, not described here.

The *prediction*, *update*, and *resample* procedures form a single iteration step; they are applied at each time step k.

Table 7.2 SIR particle filter for SOH estimation

Algorithm 2: estimation using SIR filter

Inputs: $\left\{\left(\theta_{k-1}^{d,i}, \boldsymbol{\gamma}_{k-1}^{d,i}\right), w_{k-1}^{i}\right\}_{i=1}^{N}, y_k^d$

Output: $\left\{\left(\theta_k^{d,i}, \boldsymbol{\gamma}_k^{d,i}\right), w_k^i\right\}_{i=1}^{N}$

for $i = 1$ **to** N **do**

$\boldsymbol{\gamma}_k^{d,i} \sim p\left(\boldsymbol{\gamma}_k^{d,i} \middle| \boldsymbol{\gamma}_{k-1}^{d,i}\right)$

$\theta_k^{d,i} \sim p\left(\theta_k^{d,i} \middle| \theta_{k-1}^{d,i}, \boldsymbol{\gamma}_{k-1}^{d,i}\right)$

$w_k^i \sim p\left(y_k^d \middle| \theta_k^{d,i}, \boldsymbol{\gamma}_k^{d,i}\right)$

end for

$W \leftarrow \sum_{i=1}^{N} w_k^i$

for $i = 1$ **to** N **do**

$w_k^i \leftarrow w_k^i / W$

end for

$\left\{\left(\theta_k^{d,i}, \boldsymbol{\gamma}_k^{d,i}\right), w_k^i\right\}_{i=1}^{N} \leftarrow \text{RESAMPLE}\left\{\left(\theta_k^{d,i}, \boldsymbol{\gamma}_k^{d,i}\right), w_k^i\right\}_{i=1}^{N}$

The pseudo algorithm is provided in Table 7.2.

7.3.6 RUL Prediction

The critical/failure value θ_{fail}^d of $\theta^d(t)$ must be fixed beforehand. Once the *posterior* PDF $p\left(\theta_k^d, \boldsymbol{\gamma}_k^d \middle| y_{0:k}^d\right)$ has been estimated at time step k, it should be projected in future in such a way that information about EOL at time step k, EOL_k, is obtained depending upon the actual SOH. Then, RUL at time k can be obtained as,

$$\text{RUL}_k = \text{EOL}_k - k \tag{7.48}$$

Obviously, such a projection of degradation trajectory in future has to be done in absence of measurements. Thus, this process remains outside the domain of traditional Bayesian filtering techniques. In practice, one of the efficient ways to achieve such a projection is to propagate the *posterior* PDF $p\left(\theta_k^d, \boldsymbol{\gamma}_k^d \middle| y_{0:k}^d\right)$ using the DM inspired state model (7.43) until the failure horizon θ_{fail}^d is reached. The latter may take l^d time steps so that $\theta^d = \theta_{\text{fail}}^d$ at a time $t + l^d$. This calls for computation of the predicted degradation state $p\left(\theta_{k+l^d}^d, \boldsymbol{\gamma}_{k+l^d}^d \middle| y_{0:k}^d\right)$ as [25],

$$p\left(\theta^d_{k+l^d}, \boldsymbol{\gamma}^d_{k+l^d} \middle| y^d_{0\,:\,k}\right) = \int \cdots \int \prod_{j=k+1}^{k+l^d} p\left(\left(\theta^d_j, \boldsymbol{\gamma}^d_j\right) \middle| \left(\theta^d_{j-1}, \boldsymbol{\gamma}^d_{j-1}\right)\right) p\left(\theta^d_k, \boldsymbol{\gamma}^d_k \middle| y^d_{0\,:\,k}\right) \prod_{j=k}^{k+l^d-1} d\left(\theta^d_j, \boldsymbol{\gamma}^d_j\right) \tag{7.49}$$

Obtaining the numerical value of this integral is computationally very expensive.

PFs can be employed for optimal estimation of such integrals under certain assumptions [51] reviews various methods for computation of (7.49). In [25], it is proposed that weights of the particles from time step k until $k+ l^d$ can be kept constant for l^d step ahead computation. This is based on the assumption that error generated/accumulated by keeping the weights same is negligible compared to other error sources, such as settings of process noise, measurement noise, random walk variance, and model inaccuracy [50].

In our context, as illustrated in Fig. 7.3, RUL predictions can be achieved by projecting the current SOH estimation into future [15, 16, 18, 37]. Once the particles $\left\{\left(\theta^{d,i}_k, \boldsymbol{\gamma}^{d,i}_k\right), w^i_k\right\}_{i=1}^N$, constituting the realizations of the current joint state-parameter estimate $p\left(\theta^d_k, \boldsymbol{\gamma}^d_k \middle| y^d_{0\,:\,k}\right)$ are obtained, each of the particles is propagated into future to obtain a l^d-step ahead state distribution with $l^d = 1, \ldots T^d - k$, where T^d is the time until SOH remains less than failure value, i.e., time until $\theta^d_{k+l^d} \geq \theta^d_{\text{fail}}$. For l^d-step ahead state distribution, each of the particles is propagated using the state equation of the *fault model*. Here, for the ith particle, the corresponding weight during the $l^{d,i}$-step propagation is kept equal to weight w^i_k at time of prediction k. Then, for ith particle, $\text{RUL}^i_k = k + l^{d,i} - k = l^{d,i}$ and the corresponding PDF is obtained as,

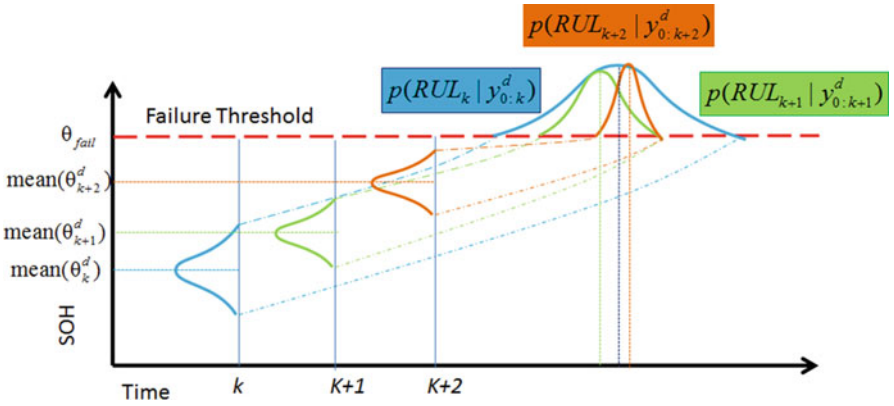

Fig. 7.3 Schematic illustration of RUL prediction process

Table 7.3 RUL prediction

Algorithm 3: RUL prediction

Inputs: $\left\{\left(\theta_k^{d,i},\ \boldsymbol{\gamma}_k^{d,i}\right), w_k^i\right\}_{i=1}^N$

Variable: l

Outputs: $\left\{\mathrm{RUL}_k^i, w_k^i\right\}_{i=1}^N$

for $i = 1$ **to** N **do**

$l = 0$

while $\theta_{k+l}^{d,i} \leq \theta_{\text{fail}}^d$ **do**

$\boldsymbol{\gamma}_{k+1}^{d,i} \sim p\left(\boldsymbol{\gamma}_{k+1}^{d,i} \middle| \boldsymbol{\gamma}_k^{d,i}\right)$

$\theta_{k+1}^{d,i} \sim p\left(\theta_{k+1}^{d,i} \middle| \theta_k^{d,i}, \boldsymbol{\gamma}_k^{d,i}\right) \quad l \leftarrow l + 1$

end while

$\mathrm{RUL}_k^i \leftarrow l$

end for

$\left\{\mathrm{RUL}_k^i, w_k^i\right\}_{i=1}^N \sim p\left(\mathrm{RUL}_k \middle| y_{0\ :\ k}^d\right)$

$$p\left(\mathrm{RUL}_k \middle| y_{0\ :\ k}^d\right) \approx \sum_{i=1}^{N} w_k^i\ \delta_{\left(\mathrm{RUL}_k^i\right)}\left(d\mathrm{RUL}_k^{\ i}\right) \tag{7.50}$$

The associated pseudo algorithm is provided in Table 7.3.

7.4 Integrated Health Monitoring

The degradation initiation is detected by BG-LFT based robust fault detection technique, as discussed in Sect. 7.3.3. The initial value of SOH of prognostic candidate is set as:

$$\theta_{t=t_d}^d \sim U\left(\theta_n^d - \Delta\theta_l, \theta_n^d + \Delta\theta_u\right)\ ; t = t_d \tag{7.51}$$

where t_d is the time when degradation is detected as fault. The associated uncertainty interval limits $[-\Delta\theta_l, \Delta\theta_u]$ decide the bounds of the uniform distribution.

The complete algorithm is shown in Table 7.4. Figure 7.4 shows the schematic description of the methodology presented in this chapter.

7.5 Evaluation Metrics

In this section, evaluation metrics are provided to assess prognostic performance. For details, readers referred to [18, 59].

Table 7.4 Integrated health monitoring of prognostic candidate

Algorithm 4: Health monitoring of θ_0^d

while *system is running* **do**
Detect the beginning of degradation using **Algorithm 1**
if *fault detection* = true **then**
//set initial conditions
$\theta_0^d \sim U\left(\theta_n^d - \Delta\theta_l, \theta_n^d + \Delta\theta_u\right)$
$\boldsymbol{\gamma}_0^d = 0$
$y_0^d = r_n^d(k)$
do SOH Estimation using **Algorithm 2**
do RUL prediction using **Algorithm 3**
end **if**
end **while**

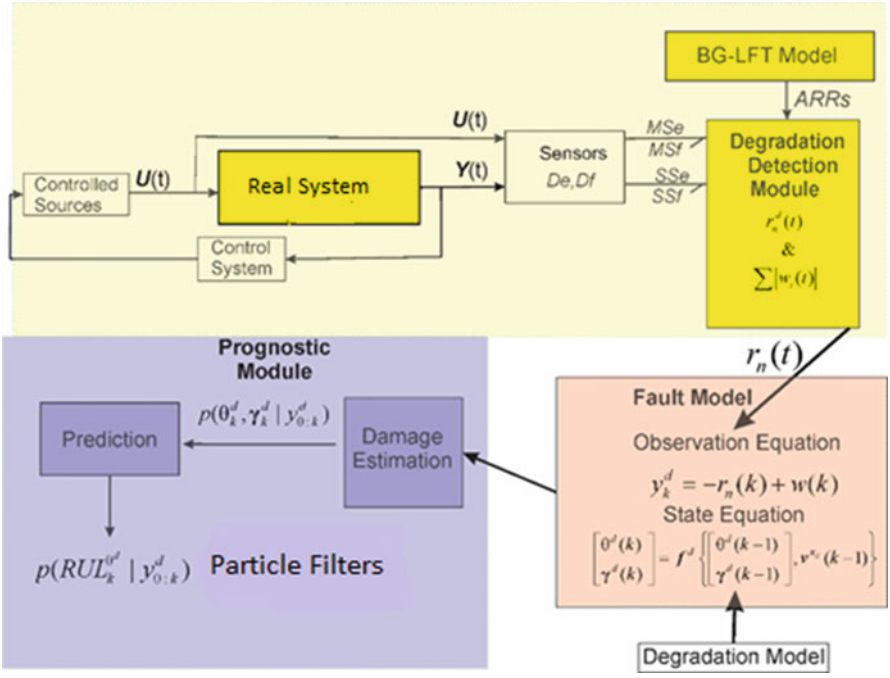

Fig. 7.4 Schematic description of the Health Monitoring Methodology

Root mean square error (RMSE) metric expresses the relative estimation accuracy as:

$$\mathrm{RMSE}_X = \sqrt{\mathrm{Mean}_k\left[\left(\frac{\mathrm{mean}(X) - X^*}{X^*}\right)^2\right]} \tag{7.52}$$

where for a specie X, X^* denotes its corresponding true value. Mean_k denotes the mean over all values of k. This metric is useful in assessing the estimation performance.

On the other hand, assessment of RUL predictions is possible if the actual RUL or RUL ground truth is known. The terms RUL ground truth and true RUL are used interchangeably in this chapter. A fairly good idea of true RUL can be obtained beforehand from the corresponding DM, under the assumption that degradation proceeds with uniform speed. Obviously, the hidden DPPs influence the actual speed and SOH. As such, in reality, true RUL can only be estimated with certain degree of belief. In this chapter, it is assumed that degradation progresses with uniform speed. As such, for evaluation purposes, true RUL is assessed from DM. A detailed discussion on this subject and RUL evaluation metrics can be found in [58, 59].

Alpha–Lambda ($\alpha - \lambda$) Metric [59] An accuracy cone is formed by choosing α such that $\alpha \in [0, 1]$, followed by generation of accuracy cone (envelope) over true RUL at time instant k, RUL_k^*, as $\left[(1-\alpha)\,\text{RUL}_k^*, (1+\alpha)\,\text{RUL}_k^*\right]$. Clearly, value of α signifies the degree of uncertainty associated with RUL_k^*, allowed for assessment of RUL predictions. Figure 7.5 shows ground truth RUL line and α cone that envelopes it. The estimated RUL PDFs must have significant amount of probability mass within the α-cone, to be accepted as "true" predictions. Then, accuracy of RUL predictions can be efficiently assessed by *relative accuracy* (RA) metric. The latter is explained by first recalling the fact that RUL predictions are obtained as PDFs (see Fig. 7.3). In this work, RUL PDFs are represented using box plot representation. As shown in Fig. 7.5, the box plot representation is capable of denoting the PDF's mean, median, 5th and 95th percentiles of distribution data, and the associated outliers. At a particular prediction instant k, the RUL prediction accuracy for θ^d is evaluated by relative accuracy (RA) metric as,

$$\text{RA}_k = \left(1 - \frac{\left|\text{RUL}_k^* - \text{Median}\; p\,(\text{RUL}_k)\right|}{\text{RUL}_k^*}\right) \tag{7.53}$$

$$\overline{\text{RA}} = \text{Mean}_k p\,(\text{RA}_k) \tag{7.54}$$

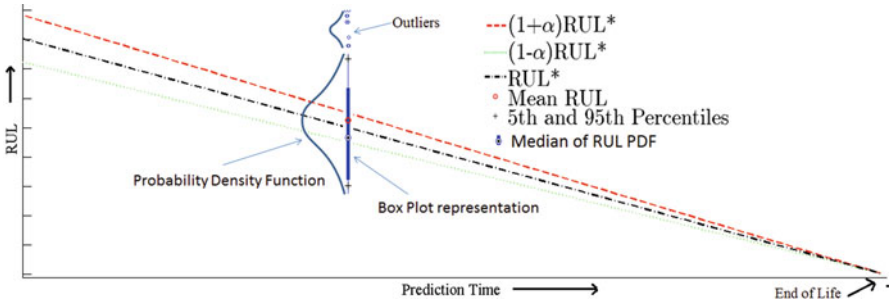

Fig. 7.5 Illustration of box plot representation and $\alpha - \lambda$ accuracy cone

where RUL_k^* denotes the true RUL at time k for θ^d. The overall accuracy is determined by $\overline{\text{RA}}$ as shown in (7.53), where RA_k is averaged over all the prediction points.

7.6 Application on Mechatronic System in Real Time

This section describes the application of the method over a mechatronic system [36] shown in Fig. 7.6. Real time implementation is achieved through 20 SIM 4C 2.1. The SOH estimation and RUL prediction algorithms are written in *Matlab Function Block* in Simulink. The embedded code is generated through Simulink Coder in Matlab2013a®.

7.6.1 Nominal System

The functional schematic model of the mechatronic system [38] is shown in Fig. 7.6. The designation of system variables and associated values are listed in Table 7.5. The system consists of the Maxon® servo motor that provides the controlled actuation (rotation) to disks (Fig. 7.7). The high stiffness transmission belt provides torque the transmission ratio of k_{belt} to the motor disk. The motor disk is connected to load disk through a flexible shaft that constitutes the drive train. The shaft is modelled as spring-damper element. The friction in the bearings of the motor disk and load disk are modelled as viscous friction. Friction arising due to belt is lumped with viscous friction coefficient at motor disk b_{Md}. The setup is equipped with motor encoder and load encoder that measure angular position of motor shaft and load disk (2000 pulses per revolution), respectively (Fig. 7.8). Angular position motor disk is obtained by dividing the motor encoder counts by belt ratio. The BG model of the

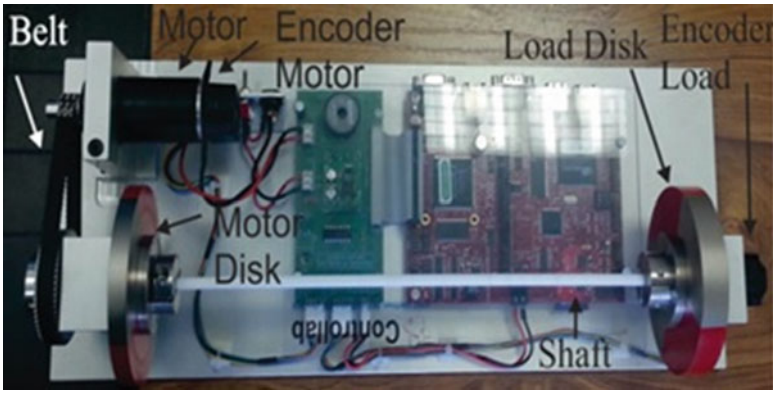

Fig. 7.6 Mechatronic torsion bar 1.0 system

Table 7.5 Details of system variables

Parameter θ	Designation	Nominal value θ_n	Multiplicative uncertainty δ_θ
k_s	Spring constant of the shaft	1.786 N m/rad	10 %
b_s	Damping coefficient of shaft	5.11×10^{-4} N m/rad	10 %
k_m	Torque constant	3.89×10^{-4} N m/A	–
k_{belt}	Teeth ratio (motor disk and motor shaft)	3.75	–
La	Rotor inductance	1.34×10^{-3} H	–
Ra	Rotor resistance	1.23Ω	–
Jm	Rotor inertia	6.76×10^{-6}kg m^2/rad	20 %
f_m	Motor friction coefficient	2×10^{-6} N m s/rad	20 %
J_{Md}	Motor disk rotational inertia	9.07×10^{-4}kg m^2/rad	10 %
b_{Md}	Viscous friction in motor disk	5.025×10^{-3} N m s/rad	20 %
J_{Ld}	Load disk rotational inertia	1.37×10^{-3}kg m^2/rad	20 %
b_{Ld}	Viscous friction in load disk	2.5×10^{-5}N m s/rad	20 %
$\text{SSf}_1 : \omega_m$	Motor velocity measurement	_	–
$\text{SSf}_2 : \omega_{\text{Ld}}$	Load disk velocity measurement	_	–
μ	Friction coefficient	0.27	10 %

nominal system in integral causality is given in Fig. 7.9. Only the monitorable part is used for analysis. The system is considered operating in feedback closed loop with Proportional-Integral (PI) controlled input voltage. The control input from PI controller (controlled variable: motor speed ω_m) modulates the input voltage MSe*:* U_{PI}.

For experiments, a mechanical lever type arrangement is fabricated as shown in Fig. 7.7 which introduces frictional torque τ_{Mech} over the motor disk by suspension of load in form of sand. The associated frictional torque is due to Coulomb friction existing between the surfaces (μ being friction coefficient). It is modulated by the suspended load M as,

$$\begin{aligned} \tau_{\text{Mech}} &= f_{\text{mech}} \times r_{\text{Md}} \\ f_{\text{mech}} &= \mu \ \text{Mg} \ \ (\omega_{\text{Md}}/\left|\omega_{\text{Md}}\right|) \end{aligned} \tag{7.55}$$

with r_{Md} as the radius of the motor disk. In the BG model, it is incorporated as non-linear resistance element R: b_{Md}. The corresponding characteristic equation becomes as,

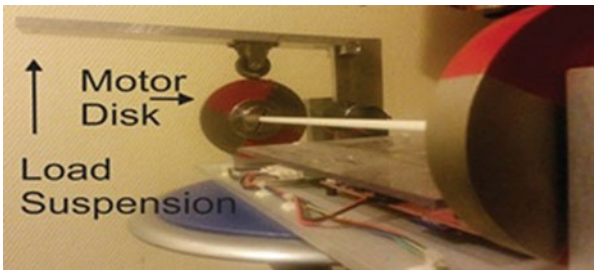

Fig. 7.7 Fabricated mechanical lever type arrangement for load (mass) suspension

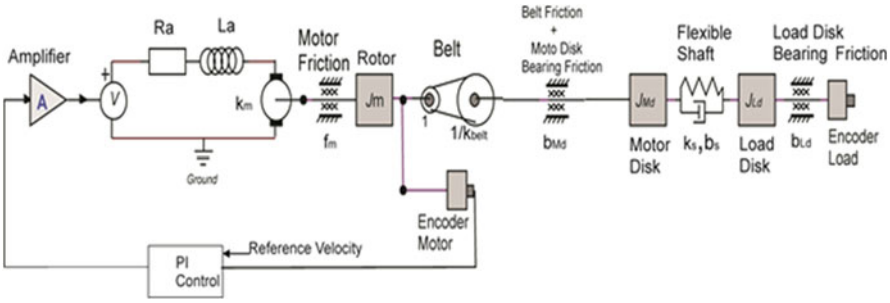

Fig. 7.8 Schematic model of the mechatronic system

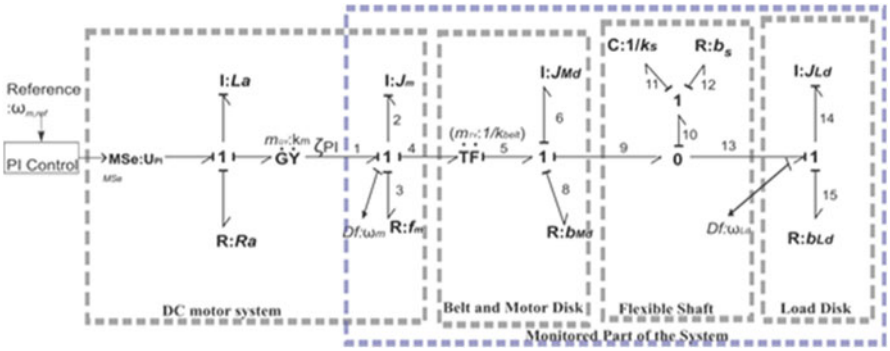

Fig. 7.9 BG model (preferred integral causality) of the nominal system

$$R = b_{\mathrm{Md}} + \mu \times M(t) \times r_{\mathrm{Md}} g / |\omega| \tag{7.56}$$

$$e_8 = R(f_8) = b_{\mathrm{Md}} \omega_{\mathrm{Md}} + \mu \times M(t) \times r_{\mathrm{Md}} g \times (\omega_{\mathrm{Md}} / |\omega_{\mathrm{Md}}|) \tag{7.57}$$

Involving only non-destructive experiments, μ is assumed undergoing no wear.

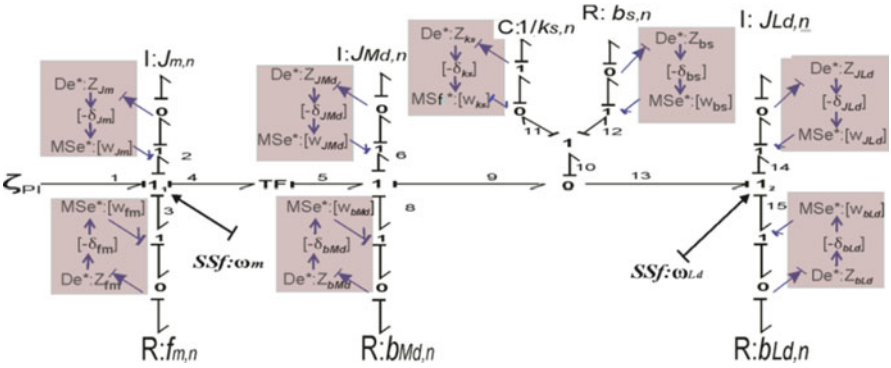

Fig. 7.10 BG-LFT model of monitorable part of the system

7.6.2 BG-LFT Model and ARR Generation

The BG-LFT model constructed in preferred derivative causality is shown in Fig. 7.10. Both the sensors are dualized and impose corresponding flows as $\boldsymbol{Y}(t) = [\mathrm{SSf}_1 : \omega_m, \mathrm{SSf}_2 : \omega_{\mathrm{Ld}}]^T$. C element remains in integral causality with the initial condition given by the flow at respective **0**-junction, provided by encoder readings as $f_{10} = f_9 - f_{13} = (\omega_m/k_{\mathrm{belt}}) - \omega_{\mathrm{Ld}}$. Moreover, electrical torque $\mathrm{MSe} : \tau_{\mathrm{PI}}$ is the PI controlled input to the monitorable part of the system and is given as:

$$\mathrm{MSe} : \tau_{\mathrm{PI}} = k_m \times i_m = k_m \times \frac{(U_{\mathrm{PI}} - k_m \times \omega_m)}{\mathrm{Ra}} \left(1 - e^{-(\mathrm{Ra}/\mathrm{La}) \times t}\right) \tag{7.58}$$

where U_{PI} is the PI controlled voltage input and i_m is the motor stator current.

Following the steps described in Sect. 7.2.3, an ARR can be generated from the detectable junction $\mathbf{1_1}$ of Fig. 7.10 as,

$$R_1 = r_1(t) + \sum w_i \tag{7.59}$$

where

$$\begin{aligned} r_1(t) = {} & \tau_{\mathrm{in}} - J_{m,n}\dot{\omega}_m - f_{m,n}\omega_m \\ & - \frac{1}{k_{\mathrm{belt}}} \left(\begin{array}{l} J_{\mathrm{Md},n} \frac{\dot{\omega}_m}{k_{\mathrm{belt}}} + b_{\mathrm{Md},n} \frac{\omega_m}{k_{\mathrm{belt}}} + \mu_n M_n g \;\; r_{\mathrm{Md}} \,\mathrm{sgn}\,(\omega_m/k_{\mathrm{belt}}) \\ + k_{s,n} \int \left(\frac{\omega_m}{k_{\mathrm{belt}}} - \omega_{\mathrm{Ld}} \right) dt + b_{s,n} \left(\frac{\omega_m}{k_{\mathrm{belt}}} - \omega_{\mathrm{Ld}} \right) \end{array} \right) \end{aligned} \tag{7.60}$$

$$\begin{aligned}
\sum w_i &= w_{Jm} + w_{fm} + w_{J_{\mathrm{Md}}} + w_{b_{\mathrm{Md}}} + w_{ks} + w_{b_s} \\
w_{Jm} &= -\delta_{J_m} J_{m,n} \dot{\omega}_m; w_{fm} = -\delta_{f_m} f_{m,n}.\omega_m; \\
w_{J_{\mathrm{Md}}} &= -\frac{1}{k_{\mathrm{belt}}} \delta_{J_{Md}} J_{\mathrm{Md},n} \frac{\dot{\omega}_m}{k_{\mathrm{belt}}}; \\
w_{b_{\mathrm{Md}}} &= -\frac{1}{k_{\mathrm{belt}}} \delta_{b_{\mathrm{Md},}} b_{\mathrm{Md},n} \frac{\omega_m}{k_{\mathrm{belt}}} + \delta_\mu \mu_n M_n g r_{\mathrm{Md}} sgn\left(\omega_m / k_{\mathrm{belt}}\right) \\
w_{ks} &= -\frac{1}{k_{\mathrm{belt}}} \delta_{k_s} k_{s,n} \int \left(\frac{\omega_m}{k_{\mathrm{belt}}} - \omega_{\mathrm{Ld}} \right) dt; \\
w_{b_s} &= -\frac{1}{k_{\mathrm{belt}}} \delta_{b_s} b_{s,n} \left(\frac{\omega_m}{k_{\mathrm{belt}}} - \omega_{\mathrm{Ld}} \right)
\end{aligned} \tag{7.61}$$

Robust thresholds over the residual can be formed as (see Sect. 7.2.3),

$$-a_1 < r_1(t) < a_1 \tag{7.62}$$

where

$$a_1 = \sum |w_i| \tag{7.63}$$

Remark Only one I-ARR has been derived in this work. This serves the purpose of demonstration. Following similar steps, another independent ARR(s) can be derived.

Figure 7.11 shows the residual profile under nominal conditions, wherein the residual is well within the envelope formed by thresholds. Figure 7.12 shows the effect of adding load (or frictional toque) in a discrete way on the system. ω_{Md} is controlled at 30 rad/s. Addition of load leads increase in frictional torque and degradation in speed. Due to action of PI controller, the motor disk speed is maintained at set reference value of 30 rad/s. However, the residual $r_1(t)$ is sensitive to the variation in PI enabled input voltage U_{PI}. As such, the residual captures the variation of disk speed due to load suspension. Saturation limit U_{PI} is reached around $t = 65$ s when the total load suspended is 1.6 Kg. Thereafter, controller is unable to compensate the change in ω_{Md}. With addition of more load thereafter ($t > 65$ s), motor disk speed decreases rapidly and stops at around $t = 70$ s. For safety reasons, the disk is stopped momentarily, after which the suspended load is removed.

7.6.3 Degradation Model: Offline Phase

The experiments performed are non-destructive in nature. Here, load in form of sand of M Kg is suspended in a uniform manner until a prefixed limit of M_{fail} is reached. In this context, $M(t)$ is treated as a system parameter under degradation, the prognostic candidate.

The experiments were conducted in two distinct phases:

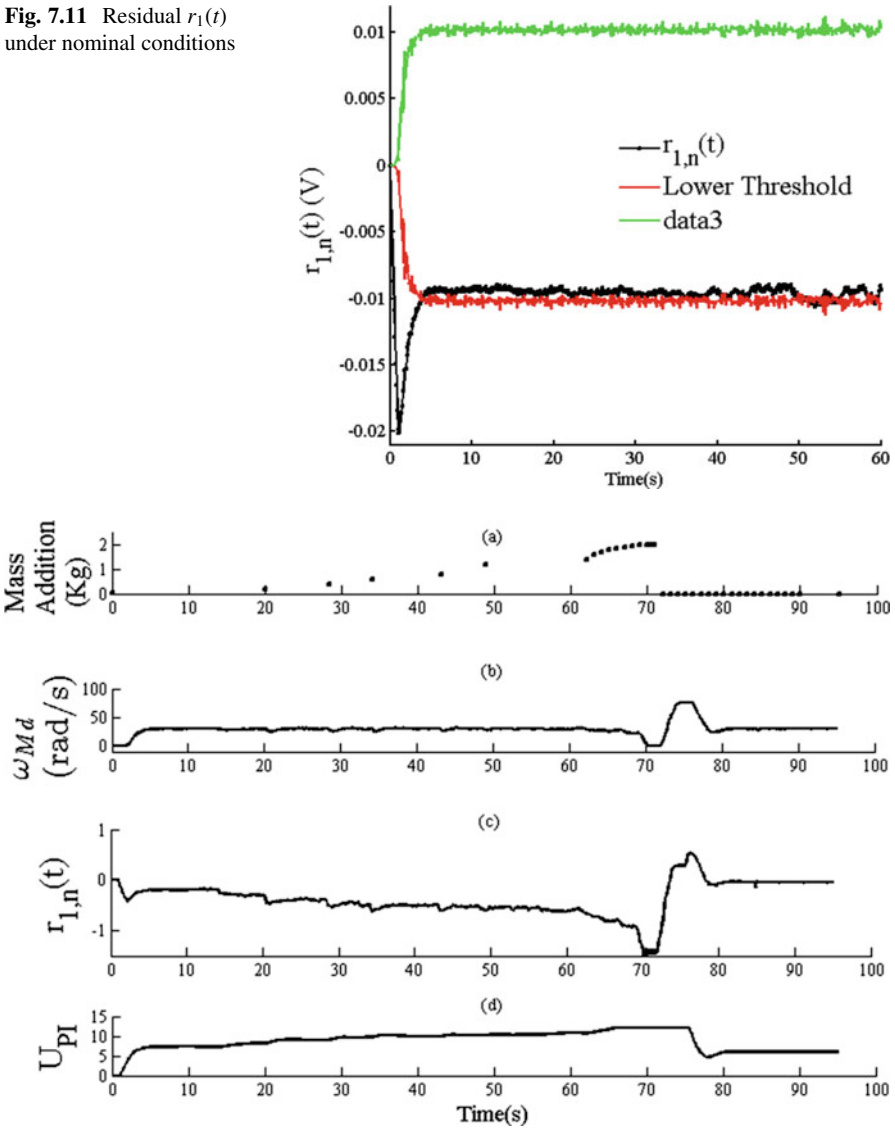

Fig. 7.11 Residual $r_1(t)$ under nominal conditions

Fig. 7.12 (**a**) Addition of load (**b**). Motor disk speed (**c**) Nominal residual $r_1(t)$ (**d**) Input voltage (PI controlled)

- Offline Phase: Mass is suspended uniformly. As explained in Sect. 7.3.1, variations of $M(t)$ are obtained from the evolution of $r_1(t)$. Then, statistical techniques such as (curve fitting) are used to obtain DM of $M(t)$.
- Online health monitoring: In real time, load is added in a similar manner under similar environmental conditions as offline phase, until the prefixed failure value

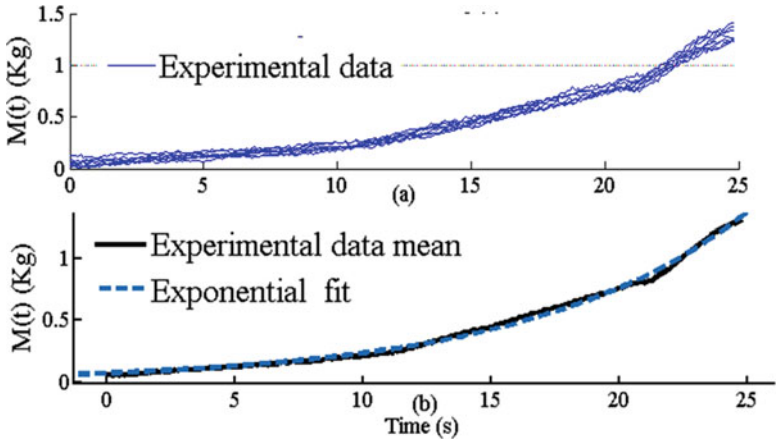

Fig. 7.13 Exponential variation of mass. (**a**) Experimental data. (**b**) Exponential fit over experimental data mean

$M(t)$ is reached. In real time, estimation of $M(t)$ and associated DPPs, and subsequent RUL predictions are obtained.

7.6.3.1 Exponential Variation of Load

Load is varied uniformly in an exponential manner. Eight experiments are carried out in total. Figure 7.13a shows the experimental data and Fig. 7.13b shows the exponential fit over the experimental data mean. This way, an exponential DM is obtained as,

$$\begin{aligned} b_{\mathrm{Md}}(t) &= g_1\left(M, \gamma_1\right) + v_{M1} \\ &= M_n \ e^{\gamma_1(t)} + v_{M1} \end{aligned} \tag{7.64}$$

where $g_1(.)$ is the DM, $\theta^d = M(t)$, DPP vector $\boldsymbol{\gamma}^d = \left[\gamma^d\right] = \gamma_1$, and normally distributed process noise $v_{M1}(t) \sim \mathcal{N}\left(0, \sigma_{M1}^2\right)$.

The DM provides an approximate true value of DPP, $\gamma_1^* = 0.05$ Kg/s. Regression residuals provide standard deviation of the process noise v_{M1}, $\sigma_{M1} = 8 \times 10^{-4}$ Kg.

7.6.4 Health Monitoring: Online Phase

In the online phase, environmental conditions are kept unaltered. It is recalled that $M(t)$ is treated as a system parameter under degradation, the prognostic candidate.

Failure value is prefixed at $M_{\text{fail}} = 1.8$ Kg. Load is varied in the similar manner until M_{fail} is reached.

7.6.5 Fault Model

In discrete time step k, the tuple $(g_1, M(t), \gamma_1)$ is formulated in state space as,

$$\begin{aligned} M_k &= M_{k-1} \times e^{\gamma_{1,k-1}\Delta t} + v_{M1,k-1} \\ \gamma_{1,k} &= \gamma_{1,k-1} + \xi_{1,k-1} \end{aligned} \tag{7.65}$$

where $\xi_{1,k} \sim \mathcal{N}\left(0, \sigma^2_{\xi_1}\right)$ is a normally distributed artificial random walk noise added to the DPP $\gamma_{1,k}$ for a suitable convergence. The magnitude of this noise should be sufficiently large for a desirable convergence of estimations and small enough for a good estimation accuracy. Usually, this noise is tuned with the help of simulations or multiple offline testing. Readers are referred to [36] for a simplified variance adaption scheme proposed in this context.

Observation equation is constructed from the ARR derived (Sect. 7.6.2) using the Theorem given in Sect. 7.3.4. The ARR : R_1 can be decomposed as,

$$R_1 : r_1(t) = r_{1,n}(t) + (M(t) - M_n) \times \frac{\partial\left(r_{1,n}(t)\right)}{\partial(M)} = 0 \tag{7.66}$$

Then, observation equation can be constructed as,

$$y_{1,k} = r_{1,n,k} + w_{1,k}(t) = (M_k - M_n)\left(\frac{\mu_n g \ r_{\text{Md}} \operatorname{sgn}\left(\omega_{\text{Md},k}\right)}{k_{\text{belt}}}\right) + w_{1,k} \tag{7.67}$$

so that the nominal part of the ARR $r_{1,n}(t)$ can be used to obtain the measurement of the state variables. Here, $w_{1,k} \sim \mathcal{N}\left(0, \sigma^2_{w1}\right)$ models noise manifesting in the residual measurements. Approximate value of σ_{w1} is determined from $r_1(t)$ values during degradation tests.

7.6.5.1 State of Health Estimation

Figure 7.14 shows the profile of residual under exponential degradation. The degradation initiation is detected when the residual goes outside the threshold envelope at around $t = 22$ s, after which prognostic module is triggered.

Estimation of SOH The estimation of suspended load $\widehat{M}$ is shown in Fig. 7.15. The estimation of SOH is performed with number of particles $N = 50$, sample time $\Delta t = 0.1$ s, initial random walk variance noise $\sigma^2_{\xi_1,k=0} = 4 \times 10^{-6}$, and standard deviation $\sigma_{w1} = 5 \times 10^{-3}$ V. For estimation of SOH, particle filter assumes

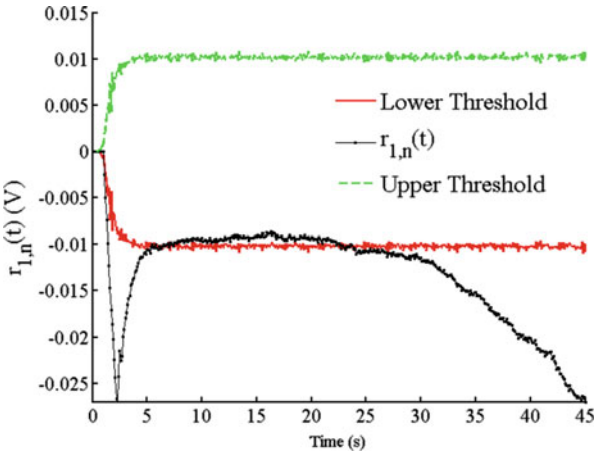

Fig. 7.14 Nominal residual $-r_{2,n}(t)$ while system is under degradation (exponential case)

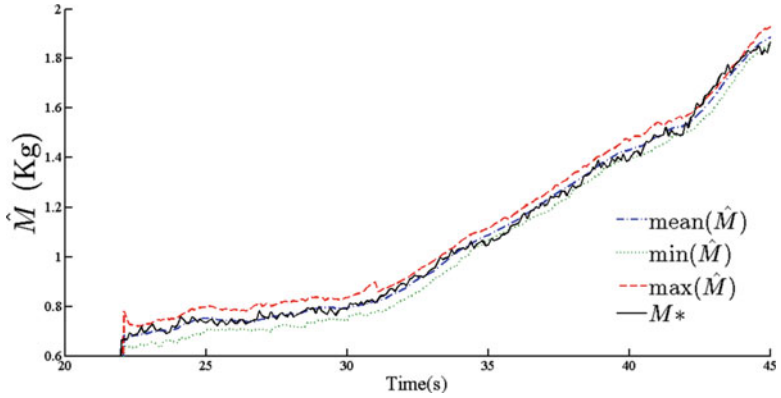

Fig. 7.15 Estimation of SOH of prognostic candidate

measurement noise variance nine times that of measurement variance σ^2_{w1}. This is done to counter sample *impoverishment* problem during the estimation process [17, 24]. The estimation is achieved with $\text{RMSE}_M = 3.78\%$. This indicates a high accuracy in estimation performance.

Figure 7.16 shows the estimation of DPP γ_1, achieved with $\text{RMSE}_{\gamma 1} = 7.6\ \%$. The convergence is achieved very quickly with large initial estimation spread. This is due to a high artificial noise variance set for the desirable quick convergence. It should be noted that RMSE_γ obtained via experiments is higher than those obtained via simulations, as the true speed of degradation γ_1^* does not remain perfectly constant in reality. Also, lesser number of particles are employed here used so that RUL predictions may be achieved in real time without significant data loss. With higher number of particles, greater accuracy may be achieved.

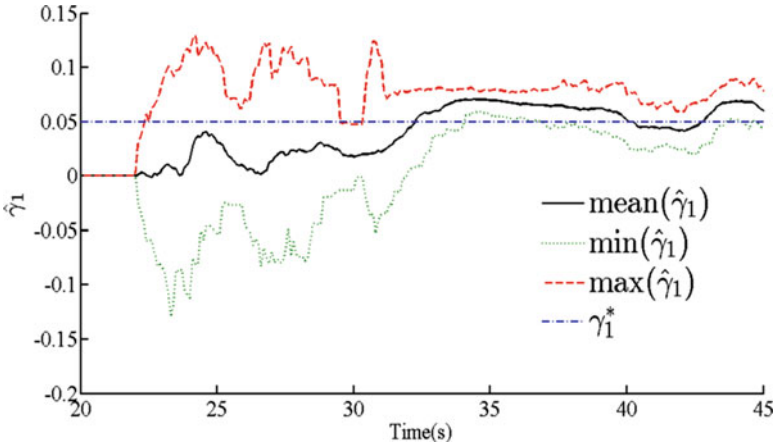

Fig. 7.16 Estimation of DPP

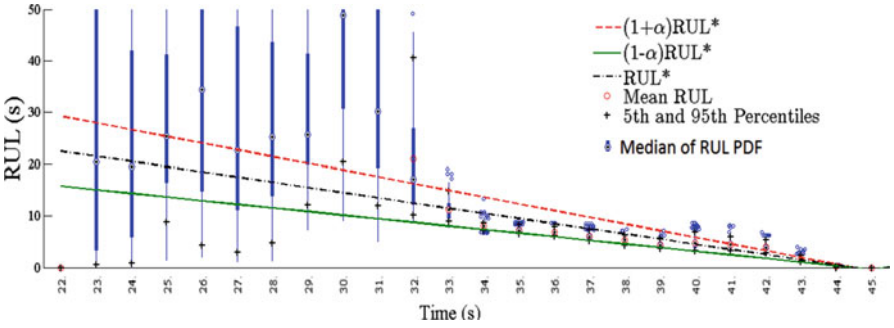

Fig. 7.17 RUL predictions

Figure 7.17 shows the RUL prediction with $\alpha = 0.2$.The RUL distributions obtained until $t = 32$ s are not good predictions and suffer with large variance spread due to a large corresponding spread in $\widehat{\gamma}_1$ (see Fig. 7.16). This makes their utility virtually null. However, after $t = 32$ s, with significant improvement in estimation of DPP, the RUL distributions are well within accuracy cone such that more than 50 % of RUL probability mass lies within accuracy cone. Ignoring the initial period of convergence, the overall prediction performance is obtained with $\overline{\text{RA}} = 97.02\%$.

7.7 Conclusions

Prognostics is the science of assessing the end of life of a system/component and prediction of the remaining useful life of the same. Due to various kinds of uncertainties that manifest in form of parametric uncertainties, environmental

conditions, sensor noises, uncertain future conditions, etc., RUL prediction becomes a very challenging issue. In this work, benefits of BG-LFT modelling based robust fault detection are integrated with the advantages of Bayesian estimation method for efficient prognostics. In particular, particle filters are exploited for optimal estimations of actual state of the prognostic candidate and subsequent RUL predictions. In this chapter, a single system parameter is chosen as the prognostic candidate and RULs are obtained with respect to that parameter. As such, the work presented here paves the future path for development of efficient system level prognostics in BG framework.

The ARR based BG-LFT technique is employed for robust detection of degradation beginning. The same ARR is then exploited for prognostic purposes. Being sensitive to the control inputs, nominal residual is able to capture the parametric degradation profile even while the system outputs remain in feedback closed loop regime. This aspect renders the approach appropriate for system level health management. Approximation of noise distribution present in residuals can be difficult or impossible, due to presence of derivative or integral terms in the ARR function arguments. As such, particle filter algorithms form the best choice in this regard as they are not restricted by non-Gaussian noises. Moreover, degradation of non-linear nature can be efficiently estimated using particle filters. Additionally, this method also demonstrates that fusion of BG-LFT framework and Monte Carlo framework leads to efficient management of various types of uncertainties. While parametric uncertainties are modelled and managed by using BG-LFT for efficient detection of degradation initiation; degradation process noise, measurement (residual) noise, etc., are efficiently accounted for, by PF for estimation of SOH and RUL predictions.

References

1. Abbas, M., Ferri, A. A., Orchard, M. E., & Vachtsevanos, G. J. (2007). An intelligent diagnostic/prognostic framework for automotive electrical systems. *Intelligent Vehicles Symposium, 2007 IEEE*. IEEE, pp. 352–357.
2. An, D., Choi, J.-H., & Kim, N. H. (2013). Prognostics 101: A tutorial for particle filter-based prognostics algorithm using Matlab. *Reliability Engineering and System Safety, 115*, 161–169.
3. An, D., Kim, N. H., & Choi, J.-H. (2015). Practical options for selecting data-driven or physics-based prognostics algorithms with reviews. *Reliability Engineering and System Safety, 133*, 223–236.
4. Arulampalam, M. S., Maskell, S., Gordon, N., & Clapp, T. (2002). A tutorial on particle filters for online nonlinear/non-Gaussian Bayesian tracking. *IEEE Transactions on Signal Processing, 50*(2), 174–188.
5. Baraldi, P., Mangili, F., & Zio, E. (2013). Investigation of uncertainty treatment capability of model-based and data-driven prognostic methods using simulated data. *Reliability Engineering and System Safety, 112*, 94–108.
6. Blischke, W. R., & Murthy, D. P. (2011). *Reliability: Modeling, prediction, and optimization* (Vol. 767). New York, NY: John Wiley & Sons.
7. Borutzky, W. (2015). Failure prognosis for hybrid systems based on ARR residuals. In W. Borutzky (Ed.), *Bond graph model-based fault diagnosis of hybrid systems* (pp. 221–233). New York: Springer.

8. Box, G. E., Jenkins, G. M., & Reinsel, G. C. (2011). *Time series analysis: Forecasting and control* (Vol. 734). Hoboken, NJ: John Wiley & Sons.
9. Bregon, A., Daigle, M., & Roychoudhury, I. (2012). An integrated framework for model-based distributed diagnosis and prognosis. *DTIC Document*.
10. Byington, C. S., & Roemer, M. J. (2002). Prognostic enhancements to diagnostic systems for improved condition-based maintenance [military aircraft]. *Aerospace Conference Proceedings, 2002. IEEE*. IEEE, vol. 2816, pp. 6-2815-2816-2824.
11. Cadini, F., Zio, E., & Avram, D. (2009). Monte Carlo-based filtering for fatigue crack growth estimation. *Probabilistic Engineering Mechanics, 24*(3), 367–373.
12. Celaya, J., Kulkarni, C., Biswas, G., Saha, S., & Goebel, K. (2011). A model-based prognostics methodology for electrolytic capacitors based on electrical overstress accelerated aging. In *Annual Conference of the Prognostics and Health Management Society (PHM),* Montreal.
13. Daigle, M. J., Bregon, A., & Roychoudhury, I. (2014). Distributed prognostics based on structural model decomposition. *IEEE Transactions on Reliability, 2*(63), 495–510.
14. Daigle, M., & Goebel, K. (2009). Model-based prognostics with fixed-lag particle filters. *Conference of the PHM Society*.
15. Daigle, M., & Goebel, K. (2010). Model-based prognostics under limited sensing. *Aerospace Conference, 2010 IEEE*. IEEE, pp. 1–12.
16. Daigle, M. J., & Goebel, K. (2011). A model-based prognostics approach applied to pneumatic valves. *International Journal of Prognostics and Health Management, 2*(2), 1–16.
17. Daigle, M. J., & Goebel, K. (2011). A model-based prognostics approach applied to pneumatic valves. *International Journal of Prognostics and Health Management, 2*(color), 84.
18. Daigle, M. J., & Goebel, K. (2013). Model-based prognostics with concurrent damage progression processes. *IEEE Transactions on Systems, Man, and Cybernetics: Systems, 43*(3), 535–546.
19. Daigle, M., Saha, B., & Goebel, K. A. (2012). Comparison of filter-based approaches for model-based prognostics. *Aerospace Conference, 2012 IEEE*. IEEE, pp. 1–10.
20. Djeziri, M., Ananou, B., & Ouladsine, M. (2013). Data driven and model based fault prognosis applied to a mechatronic system. *Power Engineering, Energy and Electrical Drives (POWERENG), 2013 Fourth International Conference on.* IEEE, pp. 534–539.
21. Djeziri, M. A., Bouamama, B. O., Dauphin-Tanguy, G., & Merzouki, R. (2011). LFT bond graph model-based robust fault detection and isolation. In W. Borutzky (Ed.), *Bond graph modelling of engineering systems* (pp. 105–133). New York: Springer.
22. Djeziri, M. A., Merzouki, R., Bouamama, B. O., & Dauphin-Tanguy, G. (2007). Robust fault diagnosis by using bond graph approach. *IEEE/ASME Transactions on Mechatronics, 12*(6), 599–611.
23. Djeziri, M., Toubakh, H., & Ouladsine, M. (2013) Fault prognosis based on fault reconstruction: Application to a mechatronic system. *Systems and Control (ICSC), 2013 3rd International Conference on*. IEEE, pp. 383–388.
24. Douc, R., & Cappé, O. (2005). Comparison of resampling schemes for particle filtering. *Image and Signal Processing and Analysis, 2005. ISPA 2005. Proceedings of the 4th International Symposium on*. IEEE, pp. 64–69.
25. Doucet, A., De Freitas, N., & Gordon, N. (2001). *An introduction to sequential Monte Carlo methods*. New York, NY: Springer.
26. Doucet, A., & Johansen, A. M. (2009). A tutorial on particle filtering and smoothing: Fifteen years later. *Handbook of Nonlinear Filtering, 12*, 656–704.
27. Engel, S. J., Gilmartin, B. J., Bongort, K., & Hess, A. (2000). Prognostics, the real issues involved with predicting life remaining. *Aerospace Conference Proceedings, 2000 IEEE.* IEEE, pp. 457–469.
28. Gebraeel, N., & Pan, J. (2008). Prognostic degradation models for computing and updating residual life distributions in a time-varying environment. *IEEE Transactions on Reliability, 57*(4), 539–550.
29. Guo, H., & Liao, H. (2015). Practical approaches for reliability evaluation using degradation data. *Annual Reliability and Maintainability Symposium*.

30. Helton, J. C. (1993). Uncertainty and sensitivity analysis techniques for use in performance assessment for radioactive waste disposal. *Reliability Engineering and System Safety, 42*(2), 327–367.
31. Herzog, M. A., Marwala, T., & Heyns, P. S. (2009). Machine and component residual life estimation through the application of neural networks. *Reliability Engineering and System Safety, 94*(2), 479–489.
32. Hu, Y., Baraldi, P., Di Maio, F., & Zio, E. (2015). A particle filtering and kernel smoothing-based approach for new design component prognostics. *Reliability Engineering and System Safety, 134*, 19–31.
33. Hitchcock, L. (2006). ISO standards for condition monitoring. In *Engineering asset management* (pp. 606–613). London: Springer.
34. Jardine, A. K., Lin, D., & Banjevic, D. (2006). A review on machinery diagnostics and prognostics implementing condition-based maintenance. *Mechanical Systems and Signal Processing, 20*(7), 1483–1510.
35. Jha, M., Dauphin-Tanguy, G., & Ould Bouamama, B. (2014). Integrated diagnosis and prognosis of uncertain systems: A bond graph approach. *Second European Conference of the PHM Society 2014-Nantes France, 2014. European Conference of the PHM Society 2014 Proceedings*, pp. 391–400.
36. Jha, M. S., Dauphin-Tanguy, G., & Ould-Bouamama, B. (2016). Particle filter based hybrid prognostics for health monitoring of uncertain systems in bond graph framework. *Mechanical Systems and Signal Processing, 75*, 301–329.
37. Jouin, M., Gouriveau, R., Hissel, D., Péra, M.-C., & Zerhouni, N. (2014). Prognostics of PEM fuel cell in a particle filtering framework. *International Journal of Hydrogen Energy, 39*(1), 481–494.
38. Kleijn, C. (2011). *20 SIM 4C 2.1 Reference Manual*. Enschede, Controllab Products B.V. ISBN 978-90-79499-14-4.
39. Klutke, G.-A., Kiessler, P. C., & Wortman, M. (2003). A critical look at the bathtub curve. *IEEE Transactions on Reliability, 52*(1), 125–129.
40. Krantz, S. G., & Parks, H. R. (2012). *The implicit function theorem: History, theory, and applications*. New York, NY: Springer.
41. Kuehl, R. W. (2010). Using the Arrhenius equation to predict drift in thin film resistors. *Proceedings CARTS Europe*, pp. 121–133.
42. Kulkarni, C. S., Celaya, J., Biswas, G., & Goebel, K. (2012). Physics based electrolytic capacitor degradation models for prognostic studies under thermal overstress. In *First European Conference of the Prognostics and Health Management Society* (Vol. 3, p. 9). Dresden.
43. Lee, J., Ni, J., Djurdjanovic, D., Qiu, H., & Liao, H. (2006). Intelligent prognostics tools and e-maintenance. *Computers in Industry, 57*(6), 476–489.
44. Li, T., Sun, S., Sattar, T. P., & Corchado, J. M. (2014). Fight sample degeneracy and impoverishment in particle filters: A review of intelligent approaches. *Expert Systems with applications, 41*(8), 3944–3954.
45. Liao, S.-H. (2005). Expert system methodologies and applications—a decade review from 1995 to 2004. *Expert Systems with Applications, 28*(1), 93–103.
46. Lu, J.-C., Park, J., & Yang, Q. (1997). Statistical inference of a time-to-failure distribution derived from linear degradation data. *Technometrics, 39*(4), 391–400.
47. Maricau, E., & Gielen, G. (2009). A methodology for measuring transistor ageing effects towards accurate reliability simulation. *On-Line Testing Symposium, 2009. IOLTS 2009. 15th IEEE International*. IEEE, pp. 21–26.
48. Medjaher, K., & Zerhouni, N. (2009). Residual-based failure prognostic in dynamic systems. *7th IFAC International Symposium on Fault Detection, Supervision and Safety of Technical Processes, SAFE PROCESS'09, vol sur CD ROM. IFAC*, p. 6.
49. Medjaher, K., & Zerhouni, N. (2013). Hybrid prognostic method applied to mechatronic systems. *The International Journal of Advanced Manufacturing Technology, 69*(1–4), 823–834.

50. Orchard, M. E. (2007). A particle filtering-based framework for on-line fault diagnosis and failure prognosis. *Georgia Institute of Technology*.
51. Orchard, M., Kacprzynski, G., Goebel, K., Saha, B., & Vachtsevanos, G. (2008). Advances in uncertainty representation and management for particle filtering applied to prognostics. *Prognostics and health management, 2008. phm 2008. International conference on*. IEEE, pp. 1–6.
52. Plett, G. L. (2004). Extended Kalman filtering for battery management systems of LiPB-based HEV battery packs: Part 3. State and parameter estimation. *Journal of Power sources, 134*(2), 277–292.
53. Rausand, M., & Høyland, A. (2004). *System reliability theory: Models, statistical methods, and applications* (Vol. 396). Hoboken, NJ: John Wiley & Sons.
54. Roychoudhury, I., & Daigle, M. (2011). An integrated model-based diagnostic and prognostic framework. *Proceedings of the 22nd International Workshop on Principle of Diagnosis (DX'11)*, Murnau, Germany.
55. Saha, B., & Goebel, K. (2009). Modeling Li-ion battery capacity depletion in a particle filtering framework. *Proceedings of the annual conference of the prognostics and health management society*, pp. 2909–2924.
56. Saha, B., Goebel, K., Poll, S., & Christophersen, J. (2009). Prognostics methods for battery health monitoring using a Bayesian framework. *IEEE Transactions on Instrumentation and Measurement, 58*(2), 291–296.
57. Saha, B., Goebel, K., & Christophersen, J. (2009). Comparison of prognostic algorithms for estimating remaining useful life of batteries. *Transactions of the Institute of Measurement and Control, 31*(3/4), 293–308.
58. Saxena, A., Celaya, J., Saha, B., Saha, S., & Goebel, K. (2009). Evaluating algorithm performance metrics tailored for prognostics. In *2009 IEEE Aerospace Conference* (pp. 1–13). IEEE.
59. Saxena, A., Celaya, J., Saha, B., Saha, S., & Goebel, K. (2010). Metrics for offline evaluation of prognostic performance. *International Journal of Prognostics and Health Management, 1*(1), 21.
60. Sikorska, J., Hodkiewicz, M., & Ma, L. (2011). Prognostic modelling options for remaining useful life estimation by industry. *Mechanical Systems and Signal Processing, 25*(5), 1803–1836.
61. Tsui, K. L., Chen, N., Zhou, Q., Hai, Y., & Wang, W. (2015). Prognostics and health management: A review on data driven approaches. *Mathematical Problems in Engineering, 2015*, 79316.
62. Vachtsevanos, G., Lewis, F., Roemer, M., Hess, A., & Wu, B. (2007). *Intelligent fault diagnosis and prognosis for engineering systems*. Hoboken, NJ: John Wiley & Sons.
63. Wu, W., Hu, J., & Zhang, J. (2007) Prognostics of machine health condition using an improved arima-based prediction method. *Industrial Electronics and Applications, 2007. ICIEA 2007. 2nd IEEE Conference on*. IEEE, pp. 1062–1067.
64. Yu, M., Wang, D., Luo, M., & Huang, L. (2011). Prognosis of hybrid systems with multiple incipient faults: Augmented global analytical redundancy relations approach. *IEEE Transactions on Systems, Man and Cybernetics, Part A: Systems and Humans, 41*(3), 540–551.
65. Zio, E., & Peloni, G. (2011). Particle filtering prognostic estimation of the remaining useful life of nonlinear components. *Reliability Engineering and System Safety, 96*(3), 403–409.